REPUBLIC OF TURKEY

YILDIZ TECHNICAL UNIVERSITY

GRADUATE SCHOOL OF SCIENCE AND ENGINEERING

FABRICATION OF POLYDIMETHYLSILOXANE MICROSTRUCTURES FOR HYDROPHOBIC SURFACES

May AKRAA

MASTER OF SCIENCE THESIS

Department of Chemical Engineering

Chemical Engineering Program

Supervisor

Prof. Dr. Hasan SADIKOGLU

Co-Supervisor

Assist. Prof. Dr. Muhammed Enes ORUC

January, 2022

REPUBLIC OF TURKEY

YILDIZ TECHNICAL UNIVERSITY

GRADUATE SCHOOL OF SCIENCE AND ENGINEERING

FABRICATION OF POLYDIMETHYLSILOXANE MICROSTRUCTURES FOR HYDROPHOBIC SURFACES

A thesis submitted by May AKRAA in partial fulfillment of the requirements for the degree of **MASTER OF SCIENCE** is approved by the committee on 17.01.2022 in Department of Chemical Engineering, Chemical Engineering Program.

Prof. Dr. Hasan SADIKOGLU	Assist. Prof. Dr. Muhammed Enes ORUC
Yıldız Technical University Supervisor	Gebze Technical University Co- supervisor

Approved By the Examining Committee

Prof. Dr. Hasan SADIKOGLU, Supervisor
Yildiz Technical University ____________________________

Doç. Dr., Nil ACARALI, Member
Yildiz Technical University ____________________________

Prof. Dr., Murat OZDEMIR, Member
Gebze Technical University ____________________________

I hereby declare that I have obtained the required legal permissions during data collection and exploitation procedures, that I have made the in-text citations and cited the references properly, that I haven't falsified and/or fabricated research data and results of the study and that I have abided by the principles of the scientific research and ethics during my Thesis Study under the title of Fabrication of Polydimethylsiloxane Microstructures for Hydrophobic Surfaces supervised by my supervisors, Prof. Dr. Hasan SADIKOGLU and Assist. Prof. Dr. Muhammed Enes ORUC. In the case of a discovery of false statement, I am to acknowledge any legal consequence.

May AKRAA

Signature

Dedicated to my family

ACKNOWLEDGEMENTS

I would like to express my deepest appreciation to my supervisors Prof. Dr. Hasan SADIKOGLU and Assist. Prof. Dr. Muhammed Enes ORUC, the completion of my dissertation would not have been possible without their support, unwavering guidance, and constructive criticism.

I would like to extend my sincere thanks to my dear friend Chemical Engineer Sevde OMEROGLU whose help and patience cannot be underestimated.

I'd like to recognize the practical suggestions and contributions that I received from Research Assistant Eda Hazal TUMER, Research Assistant Kaan YESILOVA, and other members of Oruc Lab in Gebze Technical University.

I'd also like to extend my gratitude to my family who never wavered in their support.

Finally, I'm extremely grateful to my beloved husband Muhammed Ali SAK who helped me with the schematic drawings and never let me down…

May AKRAA

TABLE OF CONTENTS

LIST OF SYMBOLS

$\sim$	Approximately
C	Carbon
CPS	Count per Second
$^\circ$	Degree
eV	Electronvolt
F	Fluorine
f	Fractional projected area of a substrate with flat surface contact angle
$>$	Greater than
HCl	Hydrochloric acid
H	Hydrogen
OH	Hydroxide
γ_{LV}	Interfacial tension of liquid-vapor interfaces
γ_{SL}	Interfacial tension of solid-liquid interfaces
γ_{SV}	Interfacial tension of solid-vapor interfaces
kV	Kilovolt
μl	Microliter
μm	Micrometer
O	Oxygen
r	Roughness factor
Si	Silicon
SiO_2	Silicon dioxide
θ_C	Static contact angle on a rough surface in Cassie-Baxter wetting model
θ_W	Static contact angle on a rough surface in Wenzel wetting model
$^\circ$C	The degree Celsius
W	Watt
θ_Y	Young's contact angle

LIST OF ABBREVIATIONS

CA	Contact angle
CAH	Contact angle hysteresis
CPS	Counts per second
CVD	Chemical vapor deposition
LBL	Layer-by-layer
PDMS	Polydimethylsiloxane
POSS	Polyhedral oligomeric silsesquioxane
PVDF	Polyvinylidene fluoride
SEM	Scanning Electron Microscopy
UV	Ultraviolet
XPS	X-ray Photoelectron Spectroscopy

LIST OF FIGURES

LIST OF TABLES

ABSTRACT

Fabrication of Polydimethylsiloxane Microstructures for Hydrophobic Surfaces

May AKRAA

Department of Chemical Engineering

Master of Science Thesis

Supervisor: Prof. Dr. Hasan SADIKOGLU

Co- supervisor: Assist. Prof. Dr. Muhammed Enes ORUC

The ability of the lotus flower, which is frequently mentioned for its superhydrophobic feature, to remain pure in an environment such as a swamp is due to the micro-sized roughness on its leaf surface. Although science and industry have done extensive work to mimic this water repellent behavior, finding a straightforward and rapid method can be challenging. For this purpose, we have improved a simple soft lithographic double-casting method to raise the hydrophobicity of polydimethylsiloxane (PDMS), which is inert, non-toxic, elastic, thermally stable, and biocompatible.

Firstly, PDMS master molds have been fabricated via the steam annealing process. Then, PDMS replicas have been produced via the double casting technique following an anti-adhesive treatment of the master molds with (tridecafluoro-1,1,2,2-tetrahydrooctyl) trichlorosilane. Another central objective of this study is to investigate the effect of different base silicone elastomer and curing agent ratios on the steam annealed master mold and replicas morphologies. The characterization of the samples has been done using Scanning Electron Microscopy (SEM), X-ray Photoelectron Spectroscopy (XPS), and contact angle measurement. The results of the morphological analysis indicate that the different ratios vary the average hole size and the surface roughness of the master mold. Also, it shows that the surface of the replica, which was produced using a steam annealed master mold with a 20:1 ratio, has lotus-leaf-like microstructures. Moreover, it has a static contact angle of more than 170° and a sliding angle of less than 2°. As XPS results confirmed the presence of fluorine on replica surfaces, it is concluded that the hydrophobic improvement is the result of both chemical treatment with fluorine silane and physically increased roughness.

Keywords: Polydimethylsiloxane, double casting, superhydrophobicity.

ÖZET

Hidrofobik Yüzeyler İçin Polidimetilsiloksan Mikro Yapılarının İmalatı

May AKRAA

Kimya Mühendisliği Anabilim Dalı

Yüksek Lisans Tezi

Danışman: Prof. Dr. Hasan SADIKOĞLU

Eş-Danışman: Dr. Öğr. Üyesi Muhammed Enes ORUÇ

Süperhidrofobik özelliği ile adından sıkça söz ettiren lotus çiçeğinin bataklık gibi bir ortamda temiz kalabilmesi, yaprak yüzeyindeki mikro boyuttaki pürüzlülükten kaynaklanmaktadır. Bilim ve endüstri, bu su itici davranışı taklit etmek için çok uğraşmış olsa da, basit ve hızlı bir yöntem bulmak zor olabilmektedir. Bu amaçla, inert, toksik olmayan, elastik, termal olarak kararlı ve biyolojik olarak uyumlu olan polidimetilsiloksanın (PDMS) hidrofobikliğini artırmak için basit bir yumuşak litografik çift döküm yöntemi geliştirdik.

İlk olarak, buhar tavlama işlemi ile PDMS ana kalıpları üretilmiştir. Daha sonra, ana kalıpların (tridekafloro-1,1,2,2-tetrahidrooktil) triklorosilan ile yapışma önleyici bir işlemden sonra çift döküm tekniği ile PDMS kopyaları üretildi. Bu çalışmanın bir diğer temel amacı, farklı silikon elastomer bazı ve kürleme ajanı oranlarının buharla tavlanmış ana kalıp ve kopyaların morfolojisi üzerindeki etkisinin incelenmesidir. Numunelerin karakterizasyonu Taramalı Elektron Mikroskobu (SEM), X-ışını Fotoelektron Spektroskopisi (XPS) ve temas açısı ölçümü kullanılarak yapılmıştır. Morfolojik analizin sonucu, farklı oranların ortalama delik boyutunu ve ana kalıbın yüzey pürüzlülüğünü değiştirdiğini göstermiştir. Ayrıca 20:1 oranında buharla tavlanmış ana kalıp kullanılarak üretilen kopya yüzeyinin lotus yaprağı benzeri mikro yapılara sahip olduğu görülmektedir. Buna ilaveten, 170°'den büyük statik su temas açısına ve 2°'den küçük kayma açısına sahiptir. XPS sonuçları, kopyaların yüzeylerinde flor varlığını doğruladığından, hidrofobik iyileştirme hem florlu silanla kimyasal işlemin hem de fiziksel olarak artan pürüzlülüğün sonucudur.

Anahtar Kelimeler: Polidimetilsiloksan, çift döküm, süperhidrofobiklik.

1
INTRODUCTION

1.1 Literature Review

In the developing world, nature has been a source of inspiration to improve sustainable solutions for problems encountered in science and industry. It contains a variety of functional mechanisms that can sometimes play a key role in the survival of a living organism including plants and animals. One of the most inspiring mechanisms is the lotus leaf surface, where the water droplets stand on the surface without wetting it. The unique hierarchical nano/microscale structures of the surface are the reason for its superhydrophobic behavior, which is frequently mentioned as the "lotus effect". In addition to the lotus leaf, many other natural surfaces also illustrate superhydrophobicity, such as butterfly wings, rose petals, water strider legs, and rice leaves [1], [2]. Superhydrophobic surface, that can repel water generally have static contact angles above 150°, and sliding angles less than 10° [2], [3].

The use of these types of water repellent surfaces is crucial in many industries. For instance, they minimize the reflection of light and prevent dust accumulation which reduces the efficiency of solar panels [4], [5]. In addition, superhydrophobic surfaces are good alternatives to hydrophilic surfaces in anti-fog applications. The reason is that although hydrophilic surfaces can eliminate fog issues, their high surface energy could easily cause contamination [6]. Also, precautions against freezing matter in aircraft, ship decks, and wind-turbine blades, etc., use superhydrophobicity phenomena since trapped air pockets in the mechanism decelerate freezing [7], [8]. Superhydrophobicity is also an essential property in anti-corrosion, drag reduction, functional textile, and lab-on-chip systems [2], [3], [9], [10].

In order to display superhydrophobic behavior, a surface should have low surface energy with nonpolar groups chemically, and more importantly, it must have roughness leading to trapping air pockets between the water droplets in the liquid phase and the solid surface [2], [11], [12]. Increasing roughness results in contact angle hysteresis (CAH) -which is an evaluation criterion of adhesion of water droplets with the surface [13]- to decrease until a minimum value is achieved, but after that, it begins to increase, which can affect adhesive properties [14]. Consequently, it is critical to optimize micro or nanoscale roughness and select proper materials to fabricate superhydrophobic surfaces.

Many techniques have been utilized to fabricate superhydrophobic surfaces. These can be categorized into three main groups: [5], [13], [15]

- Bottom-up approaches
- Top-down approaches
- Combinational approaches

In the first category, bottom-up approaches depend on adding materials onto the surfaces using chemical vapor deposition (CVD), electrochemical deposition, electrospinning, layer-by-layer (LBL) deposition, or sol−gel methods to produce rough surfaces. On the other hand, the top-down approach depends on removing/eroding material from the surfaces to obtain rough surfaces. It includes lithography, micromachining, templating, plasma etching, laser etching, and chemical etching.

Ngo et al. [1] fabricated cone-shaped structured superhydrophobic surface by ultraviolet (UV) nanosecond pulsed laser machining in combination with the polydimethylsiloxane (PDMS) casting method. Gao et al. [16] also fabricated circular micropillar structured superhydrophobic surfaces by the photolithography method. Martin and Bhushan [17] used spray coating of hydrophobic SiO_2 nanoparticles to fabricate hierarchical micro/nanoscale structures. Jia et al. [18] used the electrospraying method and fabricated cauliflower-shaped microstructures. However, high expertise for required equipment, lack of automation, and complexity of many of these processes limit their applications [11], [13].

On the contrary, polymer molding is rapid, simple, and valuable in mass production [1]. Many polymers can be ideal choices to produce superhydrophobic surfaces, especially for non-planar ones. Among them, PDMS is extensively used due to its inherent hydrophobicity, low surface energy, chemical inertness, thermal stability, biocompatibility, and flexibility [1], [19]. The contact angle value of a flat PDMS surface is approximately 110° [16]. As a consequence, with fabricating microstructured PDMS surfaces, higher contact angle values can be achieved without additional treatments.

For this purpose, in this thesis, we present a straightforward soft lithographic double casting method of PDMS to improve its surface water repellency. Soft lithography depends on a set of methods that benefit from a patterned elastic polymer as a mold to develop microstructures and micropatterns rather than employing a hard photomask as in photolithography [20]. Even though soft lithography has superior advantages such as low cost, simple setup, and high outputs, it generally needs another method such as photolithography or e-beam lithography to fabricate the master molds [21].

1.2 Objective of the Thesis

The key factor in water repellent superhydrophobic surfaces is to create hierarchical roughness. However, creating microscale superhydrophobic water repellent structures can be challenging and time-consuming. Soft lithographic PDMS microstructure fabrication generally pre-requests other complex and expensive methods to create the master molds.

This thesis aims to present a simple two-step procedure soft lithographic double-casting approach to fabricate superhydrophobic PDMS microstructures. Firstly, we intend to utilize a facile technique, steam annealing process for producing the master molds. This method forms micro holes within the PDMS master surface by elevated temperature, pressure, and moisture. The second goal is to fabricate replicas with micropillars using the micro-holed master molds. However, before double casting, anti-adhesion treatment is going to be applied. In addition to that, we aim to investigate the base silicon elastomer and curing agent ratio for the master fabrication that can affect the superhydrophobicity of produced replica.

1.3 Hypothesis

If an inherent hydrophobic surface consists of an appropriate roughness, air pockets will be trapped between the nano/microstructures and the water droplet exhibiting the Cassie Baxter wettability model. Hence, we hypothesize that utilizing steam annealed micro-holed master molds in fabricating microstructured PDMS replicas will give the surface the required roughness to achieve a higher static contact angle and lower sliding angle which means to develop its superhydrophobic behavior.

2
BACKGROUND

2.1 Superhydrophobicity

Latin words hydrophobicity, hydrophilicity, superhydrophobicity, and superhydrophilicity are terminologies related to the wettability of a solid surface. In other words, as “hydro” means water and “phobos” means “fear”, hydrophobicity and superhydrophobicity terminologies are related to water-fearing and hydrophilicity, and super hydrophilicity represent water-loving behaviors as considering "philic" means love.

Experimental measurement of a water contact angle (CA) is used to characterize solid surface wettability. A surface with CA larger than 90° is considered hydrophobic. On the other hand, a hydrophilic surface has a lower CA than 90° [22]. For a surface to be superhydrophobic, it must have a water contact angle greater than 150°, as well as a low contact angle hysteresis (preferably below 10°) and/or a low sliding angle [2]. Figure 2.1 shows the main difference between hydrophilicity, hydrophobicity, superhydrophilicity, and superhydrophobicity.

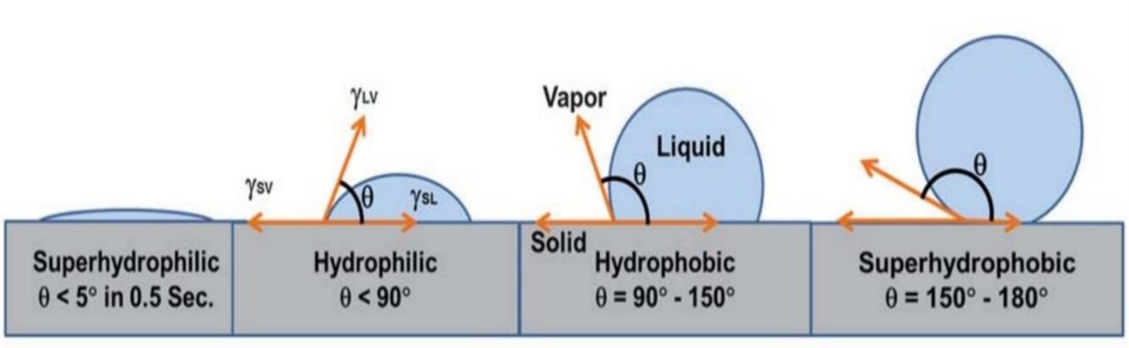

Figure 2.1 The difference between hydrophilicity, hydrophobicity, superhydrophilicity and superhydrophobicity [23]

2.2 Natural Superhydrophobic Surfaces: Lotus Leaves and Rose Petals

Lotus plant (*Nelumbo nucifera*) has purity symbol in far east cultures due to its ability to stay immaculate even in a muddy environment. Researchers examining the lotus plant, which has a self-cleaning feature, discovered that there are basically two reasons for this. First, the lotus leaf is covered by a waxy epicuticular surface, and it is an inherently hydrophobic surface. Second, it has both micro and nano-scaled stratified roughness (Figure 2.2) or, in other words, hierarchical irregular roughness [24]. While the water contact angle of a flat epicuticular wax layer, which is structurally composed of hydrocarbon with low surface tension, is about 110°, this value can go up to 164° thanks to the roughness of 10 μm and 100 nm; meanwhile, it lowers the hysteresis giving a sliding angle of less than 4° [25].

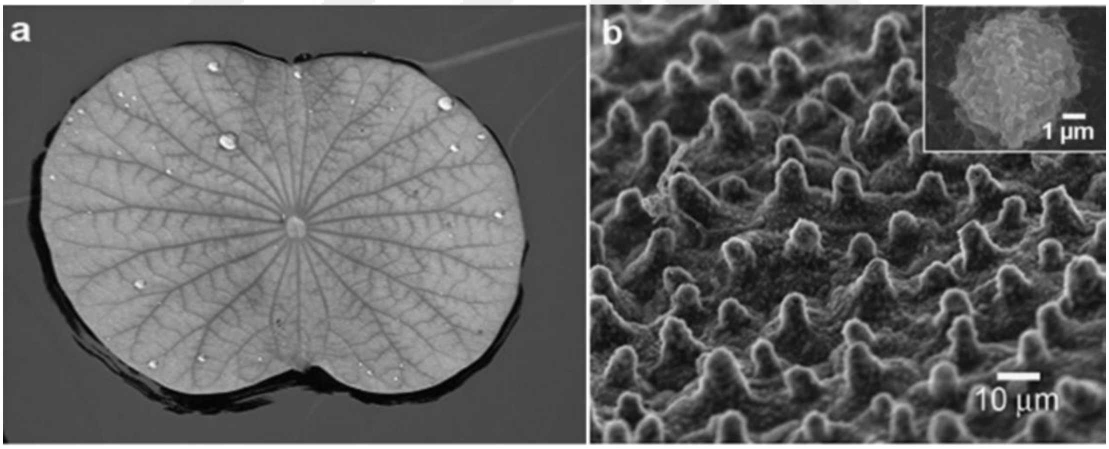

Figure 2.2 A lotus leaf on water and an environmental scanning electron microscopy image of its surface [26]

Rose petal is another example of natural superhydrophobic surfaces. However, unlike lotus leaves, it does not repel the dripping water. On the contrary, water droplets stick to the petal. These adhering drops eventually evaporate, providing the moisture needed for its flourish. Although the water droplet has a contact angle value of 152° on this surface [27], the reason for its adhesion is that the water completely penetrates into the micro-sized grooves of the hierarchical roughness and, therefore, the liquid-solid interface contact area remains high since air pockets are not trapped. As a result, it causes high contact angle hysteresis and exhibits an intermediate wetting modulus between the Wenzel and Cassie-Baxter wetting modulus; this is called the "petal effect" [28], [29].

2.3 Wettability Models

Wettability is one of the most significant qualifications of a solid surface. In 1805, Thomas Young came up with a model that is the essential stone in defining wetting phenomena that occur between a liquid and a solid [30]. In the Young model, the contact angle at which a liquid touches a flat, homogeneous, ideal solid surface is represented by the following equation (2.1):

$$\cos\theta_Y = (\gamma_{SV} - \gamma_{SL})/\gamma_{LV} \tag{2.1}$$

where θ_Y is the Young's contact angle, and γ_{SV} , γ_{SL}, γ_{LV} are the interfacial tensions of solid-vapor, solid-liquid, and liquid-vapor interfaces, respectively. Young concluded that as the surface becomes more repellent, the water contact angle increases. On the contrary, when the droplet splays and wets the surface, it displays a low contact angle [30].

For non-ideal surfaces, there are two wetting models may occur, the Wenzel model and the Cassie-Baxter model [2].

In the Wenzel wetting model, the liquid penetrates entirely into the grooves between the roughness of the surface. Equation (2.2) shows the Wenzel's equation [2]:

$$\cos\theta_W = r(\gamma_{SV} - \gamma_{SL})/\gamma_{LV} = r\cos\theta_Y \tag{2.2}$$

where r is the roughness factor, θ_W is the static contact angle on a rough surface, and $\theta_Y$is the contact angle on a flat surface. The roughness factor is defined as the ratio between the actual surface are and the projected one.

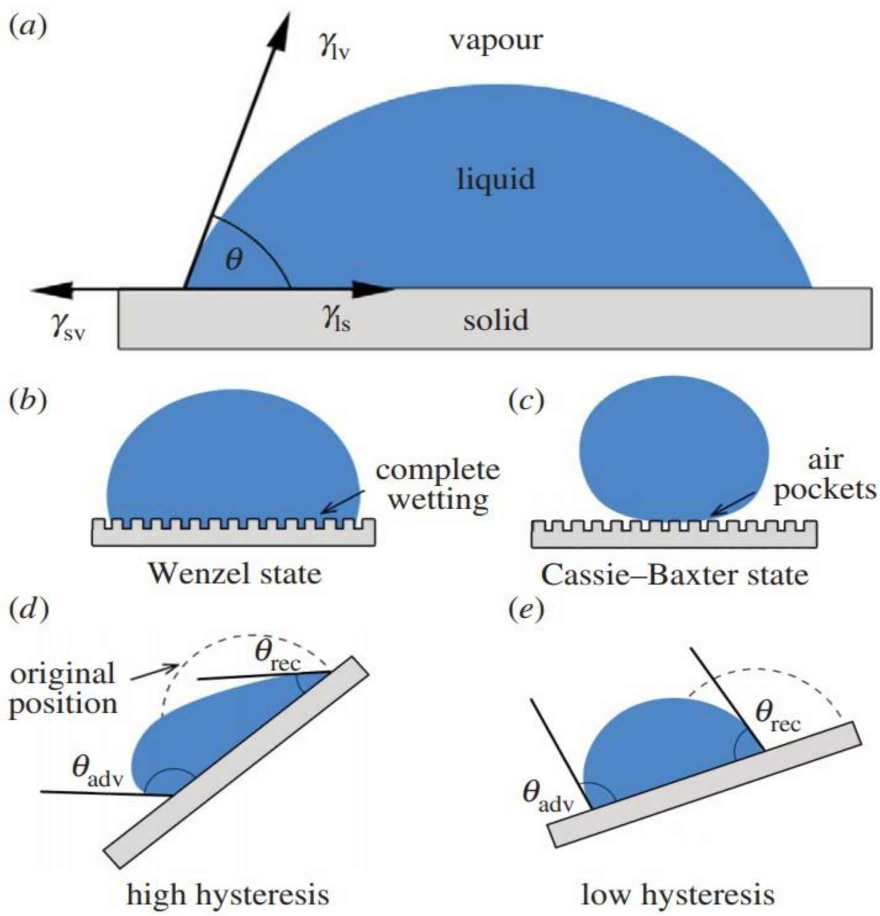

Figure 2.3 The mehanism of wetting models [22]

In the Cassie-Baxter model, air pockets are trapped between the solid and the liquid. Cassie-Baxter model gives a more repellent surface because of partial resting of the water droplet on air. Equation (2.3) shows the Cassie-Baxter equation [2]:

$$\cos\theta_C = f\cos\theta - (1 - f) \tag{2.3}$$

where θ_C is static contact angle on a rough surface in this wetting model, f is the fractional projected area of a substrate with a flat surface contact angle θ.

Unlike an ideal surface in Young's wetting model, all natural surfaces have tropological roughness even in atomic size. When a water droplet slides on these surfaces, it faces hysteresis due to the surfaces' roughness and/or chemical heterogeneity [14]. Figure 2.3 shows the mechanism of each wetting model.

Contact angle hysteresis is the difference between the advancing angle and the receding angle [2]. Low contact angle hysteresis refers to the low adhesion of the water droplet on the surface so that it is an important criterion for superhydrophobicity [22]. Another criterion is sliding angle; even if it has a similar physical meaning to contact angle hysteresis, it is measured as a weighted water droplet begins to move on a tilted plate [2].

2.4 Fabrication Methods of Superhydrophobic Surfaces

To obtain a superhydrophobic surface, the roughness of a low surface energy surface must be increased, or the surface energy of a rough surface must be reduced. If the roughness of a surface is inadequate and does not have low surface energy, then both processes must be applied [15].

In terms of roughness, photolithography, etching, and laser ablation methods are used to produce rough surfaces with regular structures, while methods such as electrospinning, layer-by-layer, spin coating, spray coating, dip coating, and casting are used for irregularly rough surfaces [28].

Photolithography is a method that is widely used in the production of rough surfaces with controllable regular geometries. The basic principle of this method, which consists of many stages, is related to the transfer of geometry by exposing a material with light sensitivity covered with a patterned mask of the desired size to ultraviolet (UV) irradiations [31]. For instance, Gao et al. [16] utilized this technique to fabricate circular micro pillared PDMS surfaces to investigate dimensional effects on Cassie-Baxter and Wenzel transition state (Figure 2.4). They achieved fabricating a superhydrophobic PDMS surface with CA close to 170° without additional treatments. However, this method requires cleanroom processing which limits its applications.

Etching is a method used for the fabrication of isotropic or anisotropic 3-dimensional micro/nanostructures. Dry etching refers to the scraping of material from the surface by utilizing the physicochemical reaction of appropriate gases, while wet etching uses a chemical liquid for that. Although this method is preferable to fabricate highly complex roughness, chemical contamination is just one of its disadvantages [28], [31].

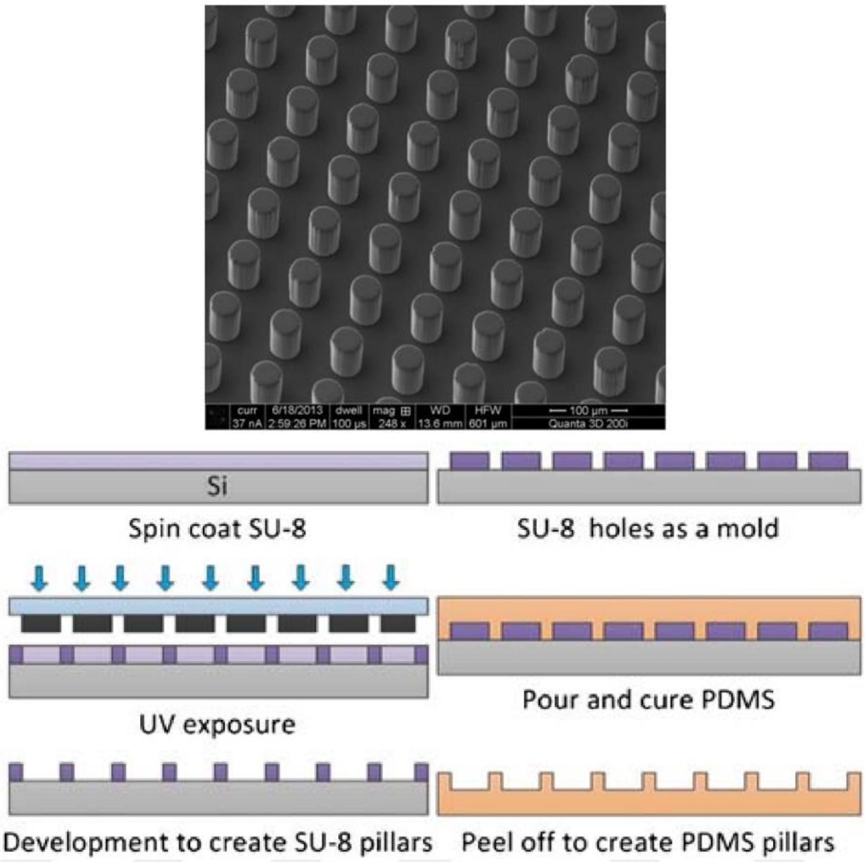

Figure 2.4 Circular micropillared PDMS surface produced by photolithography method [16]

The laser ablation method is used to obtain a superhydrophobic surface either directly to increase the roughness of a surface by ablating a surface or indirectly to texture the main template in the production of superhydrophobic polymers [11], [32]. There are two types of lasers in these ablation processes, long-pulsed laser and short-pulsed laser. Although long-pulsed laser, also known as nanosecond lasers, is widely used industrially, it gives low-quality shapes because it roughly carves the edges. In fact, more controllable cavities and edges are desired to obtain hierarchical microstructured surface. On the other hand, there are two types of short-pulse lasers, femtoseconds and picoseconds. Femtoseconds allow for much ultra-higher quality ablations. However, picoseconds are more widely used because femtoseconds are very costly and probable to break down [11], [28]. Tang et al. [32], employed UV pulsed laser to produce a superhydrophobic metal surface directly. Thereby, they enhanced the water CA of an ablated brass surface from 110° to 161°. As seen in Figure 2.5, Ngo et al. [1]

used UV laser ablation to texture an aluminum template for the PDMS casting process. They investigated the spacing size effect between the cone-shaped microstructures in terms of transmittance.

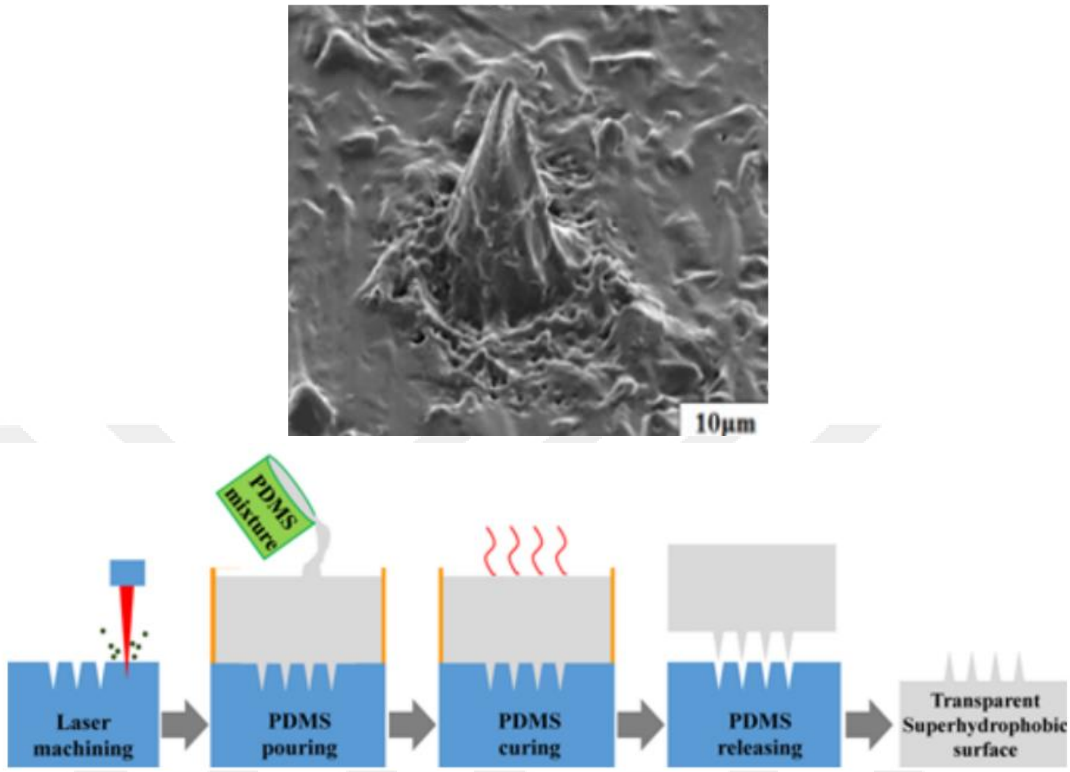

Figure 2.5 Transparent superhydrophobic surface produced by laser ablation [1]

Electrospinning and electrospraying, which are used widely in the production of superhydrophobic membranes, are the methods based on spraying a syringe containing a polymer solution with a certain flow rate at high voltage to a collection plate [15]. For instance, Jia et al. [18] synthesized polydimethylsiloxane-polyhedral oligomeric silsesquioxane (PDMS-POSS) nanocomposites and electrosprayed the polymer solution with polyvinylidene fluoride (PVDF) producing a cauliflower-shaped microstructured membrane surface with a water contact angle of 166° (Figure 2.6).

The layer-by-layer (LBL) method refers to coating more than one layer onto the surface. In this method, a stable multilayered film is formed by utilizing the electrostatic interactions of the layers with a sequential coating of nanosized polyanions and polycations [15], [28]. For example, Yang et al. [33] fabricated a superhydrophobic paper having a water CA of approximately 162° by the LBL assembly of cationic starch and sodium alginate involving trichloromethylsilane treatment.

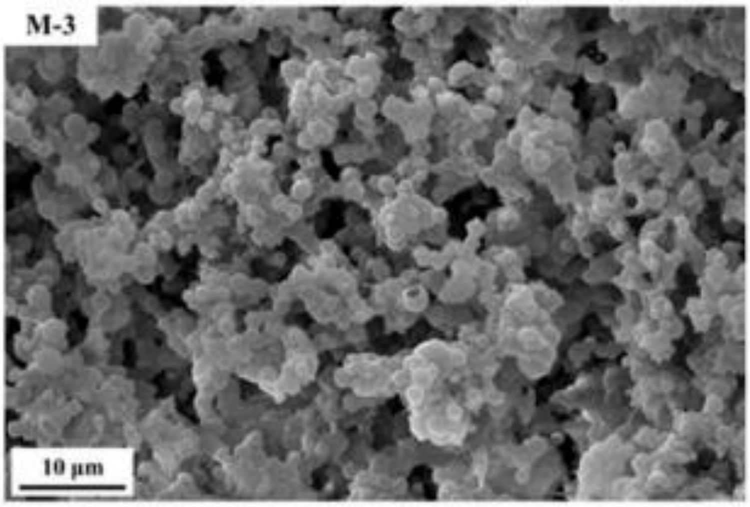

Figure 2.6 Electrosprayed superhydrophobic cauliflower-shaped PDMS-POSS surface [18]

Spin coating and spray coating are extensively used in superhydrophobic fabrications. Spin coating depends on rotating the substrate to spread a solution onto a surface uniformly. Long et al. [34] spin coated PDMS solution onto a rough aluminum surface in order to produce a strong water repellent surface that can regain its superhydrophobicity by annealing at 350 °C even after physical and chemical damages. Celik et al. [35] also fabricated a mechanically robust superhydrophobic surface with water CA of 175° by one-step spray coating of carnauba wax with hydrophobic silica nanoparticles using chloroform as a solvent.

Dip coating methods involve immersing a substrate into a specific solution to increase its roughness. Lee et al. [36] created a surface using polylactic acid filaments via 3D printing, then dip-coated in a system consisting of hydrophobic silica nanoparticles and methyl ethyl ketone to add roughness to the surface.

The soft lithography method is one of the top-down approaches in fabricating microstructured surfaces. It is called "soft" because of the use of an elastomer. Soft lithography has many advantages such as being simple, inexpensive, and workbench friendly as there is no need for a cleanroom. Also, the use of elastomers makes it possible to produce flexible rough surfaces. The soft lithographic method comprises imprinting, transferring, and molding. One of the fundamentals in soft lithography is preparing a master mold or a stamp to replicate or transfer the design [37]. For instance, after pouring prepolymer on a fresh lotus leaf and making a master mold, Liu et al. [38] used it to shape different substrates with the imprinting method. The water contact angle value they reached is approximately 155°.

2.5 Application of Superhydrophobic Surfaces

One of the most desired properties of superhydrophobic surfaces is the self-cleaning feature. Deserts are the preferred areas for installing solar panels, as they provide a large surface area as well as being the place where the sun hits the most. However, due to the problem of dust accumulation, the energy efficiency of these solar panels can be reduced by 60% [4]. Therefore, developing self-cleaning solar panels is an area of interest for many scientists (Figure 2.7).

Figure 2.7 Dusty and clean solar panels [39]

For instance, Kang et al. [40] used a combinational approach of soft lithographic replica molding and Argon ion surface treatment to fabricate anti-reflective and self-cleaning solar cells with a pyramidal array of 30 μm width and 15 μm height. The results show that the solar cells had 14.01% power conversion efficiency, 157° and 7° of water contact angle, and sliding angle, respectively.

Superhydrophobic surfaces also can be a solution for icing that can cause severe problems in airplanes (Figure 2.8), ships, wind turbines, telecommunications equipment, roads, etc. Although methods such as defrosting by heating and adding chemical additives work to prevent this, superhydrophobic surfaces that do not require any additional treatment are seen as a potential solution. For example, Liu et al. [8] developed a superhydrophobic coating of polyacrylic acid-based resin material with modification of SiO_2 nanoparticles for anti-freezing application.

Figure 2.8 Icing problem in an aircraft

Another area where superhydrophobic surfaces are widely used is fabricating anti-corrosion metallic surfaces such as aluminum [41], [42], magnesium [43], steel [44] surfaces, etc. In addition, much research focused on developing superhydrophobic functional textiles. For instance, Shao et al. [45] were inspired by polar bear hair and produced thermal insulating superhydrophobic textile. Also, Ye et al. [46] created an antibacterial waterproof textile.

Another field of superhydrophobic applications is water-oil separation. For instance, Sow et al. [47] synthesized a coating with fly ash and vulcanizing silicone. The separation efficiency of the coating was higher than 99%. As seen in Figure 2.9, water cannot cross the superhydrophobic coating; however, oil can penetrate easily.

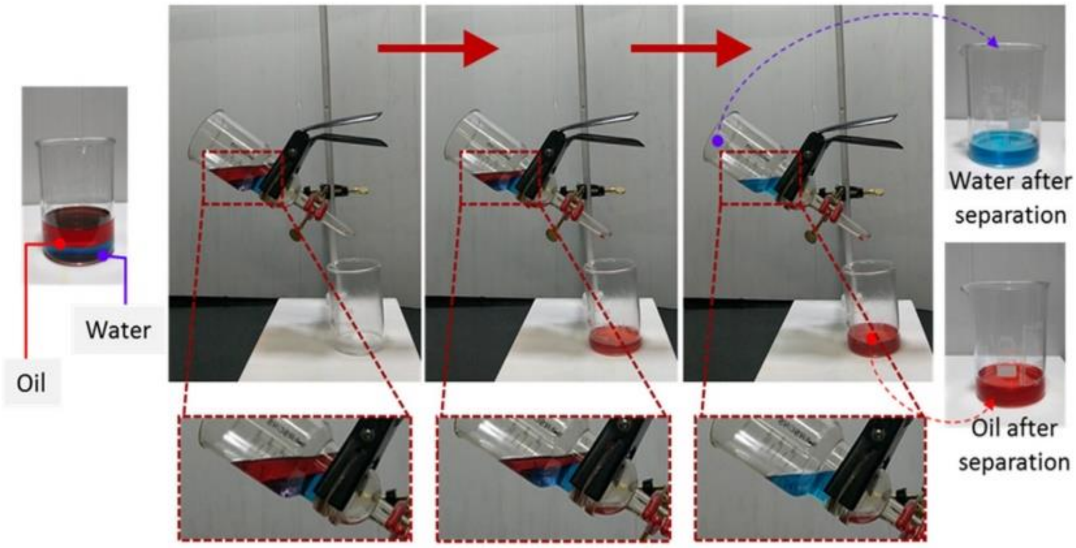

Figure 2.9 Water-oil separation by superhydrophobic coating [47]

2.6 PDMS Steam Annealing Process

The conventional technique to obtain PDMS is by mixing a viscous monomer silicone base elastomer and a crosslinker curing agent with a 10:1 ratio (wt/wt) followed by degassing the air bubbles and curing at different temperatures and durations.

The principle of the PDMS steam annealing process is to boil water in a pressurized chamber and expose the formed hot water vapor on the prepolymer resulting in holes formation on the surface and rapid curing. The pressure and annealing time could affect the depth of the holes [48].

In 2012, Jeong et al. [48] obtained a porous PDMS surface (Figure 2.10) via steam annealing the uncured polymer. In their study, after spinning uncured PDMS on a Si wafer, a SU-8 mask was placed on it and then annealed in a steam chamber (Figure 2.11) for 5 minutes. In this way, a perforated structure was obtained to be used in producing a flexible electronic circuit. They also showed that there is no difference between the molecular structures of PDMS that cured on a hot plate and steam annealed PDMS. On the other hand, Jung et al. [49] utilized an autoclave instrument to steam annealing PDMS prepolymer for 10 minutes and obtained micro holes with 17 μm depth. In 2017, Yun et al. [50] also fabricated a porous PDMS surface by steam annealing for 30 minutes.

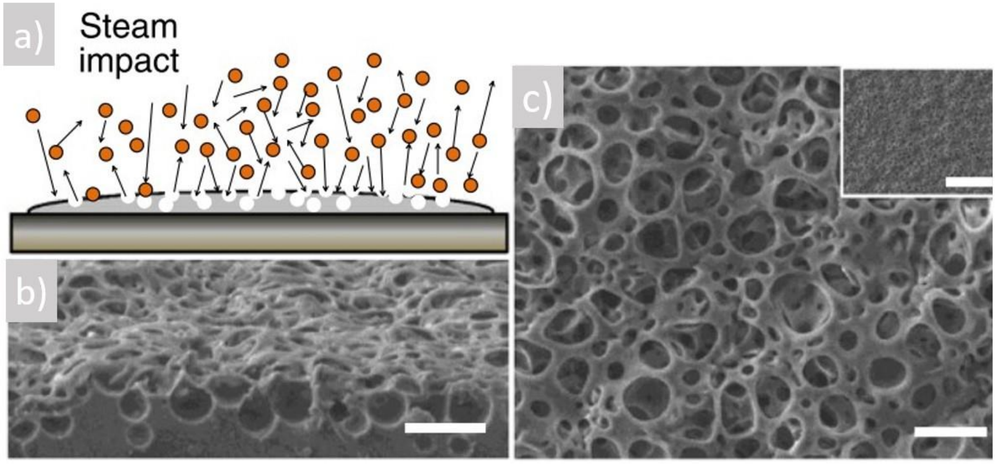

Figure 2.10 A schematic diagram of steam annealing process (a), a cross-section (b) and a top (c) views of scanning electron microscopy images of steam annealed PDMS [48]

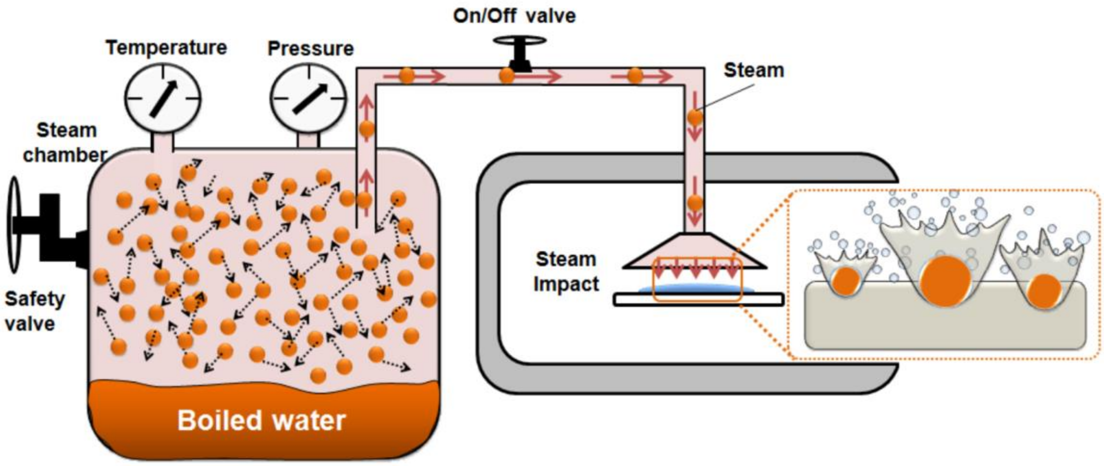

Figure 2.11 Steam annealing process used for fabrication porous PDMS surfaces [48]

3
EXPERIMENTAL METHOD

3.1 Materials Used

All chemicals used in this study are listed in Table 3.1.

Table 3.1 Chemicals used through the study and their suppliers

Chemical	Chemical Formula	Supplier
Polydimethylsiloxane (PDMS)	$(C_2H_6OSi)_n$	Dow Corning (Sylgard 184)
(Tridecafluoro-1,1,2,2-tetrahydrooctyl) trichlorosilane, 97% .	$C_8H_4Cl_3F_{13}Si$	ABCR (AB111444)
Ethanol	C_2H_6O	ISOLAB Chemicals

3.2 Soft Lithographic Method

3.2.1 Preparation of PDMS Master Molds by Steam Annealing Process

The first step in the soft lithographic replica molding method is fabricating a master mold. The steam annealing process was selected in our study to grow microholes on PDMS master molds due to its low cost and simplicity. Figure 3.1 illustrates the steam annealing process. PDMS prepolymers were prepared with different ratios to investigate the effect of silicone elastomer and curing agent ratio on surface morphology.

Firstly, base silicone elastomer and curing agent were mixed at 5:1, 10:1, and 20:1 (wt/wt) ratios and cast on glass petri dishes. Then, each uncured polymer was kept in a vacuum desiccator for 45 minutes to remove the air bubbles formed during the mixing process. After that, it was placed in an autoclave instrument (Hirayama HVE-50 autoclave) for a pressurized steam annealing process at 120 °C for 20 minutes. Figure 3.2 shows the autoclave instrument. Finally, annealed PDMS master mold was dried out on a hot plate at 70 °C. The prepared steam annealed PDMS master molds were coded as shown in Table 3.2.

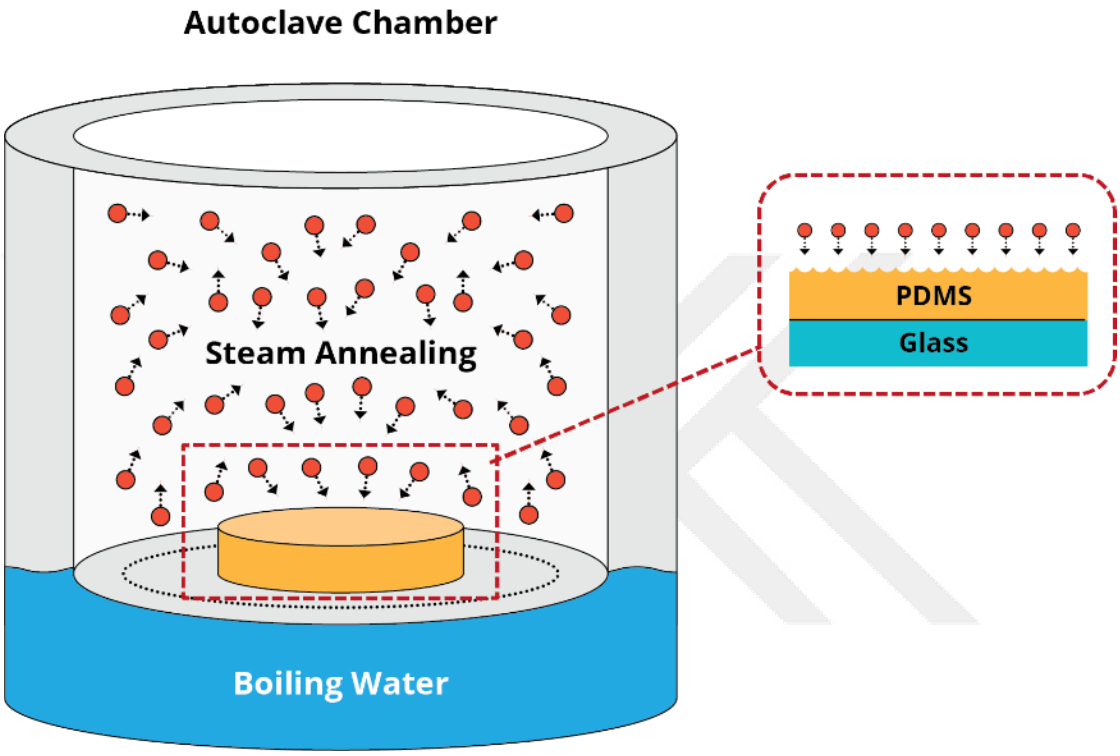

Figure 3.1 Steam annealing process

Table 3.2 Coding of the master molds prepared through steam annealing of PDMS

Sample Code	Meaning of the Codes
M5	PDMS master mold with 5:1 (wt/wt) ratio of base silicone elastomer to curing agent
M10	PDMS master mold with 10:1(wt/wt) ratio of base silicone elastomer to curing agent
M20	PDMS master mold with 20:1 (wt/wt) ratio of base silicone elastomer to curing agent

Figure 3.2 Hirayama HVE-50 autoclave

3.2.2 Anti-adhesion Treatment onto PDMS Masters

It is necessary to perform an anti-adhesion treatment on the master molds for double casting of PDMS to prevent permanent adhesion between PDMS-PDMS layers and easily separate them. In this study, (Tridecafluoro-1,1,2,2-tetrahydrooctyl)trichlorosilane; in other words, fluoro silane gas deposition was applied to form an anti-adhesive protective layer [51]–[55]. This fluoro silane reacts with a hydroxyl group on a plasma treated PDMS surface, forming self-assemblies and covalent bonds between silicon and oxygen atoms.

To enable the bonding of fluoro silane on the surfaces during gas deposition, master molds were activated by oxygen plasma generated using airflow for 2 minutes (~30 W, Harrick Plasma Cleaner, Chemical Engineering Department, Gebze Technical University). Figure 3.3 shows the plasma cleaner instrument that was utilized in this thesis.

Figure 3.3 Harrick Plasma Cleaner

Oxygen plasma activates the PDMS surface and forms polar groups, which are C-OH and mainly Si-OH, that cause a hydrophilic effect [56], [57]. Before oxygen plasma activation, the master molds were sonicated with ethanol and water for 2 minutes, respectively, to remove possible contamination. After the plasma treatment, each of the master molds was quickly placed in a plastic Petri dish to avoid losing the activation effect. 25 µl of fluoro silane was dropped on the cover of the Petri dish with the help of an automatic pipette. The cover was closed and waited for 80 minutes to allow fluoro silane to evaporate and bond on the activated surfaces. Figure 3.4 illustrates the mechanism of the mentioned protocol.

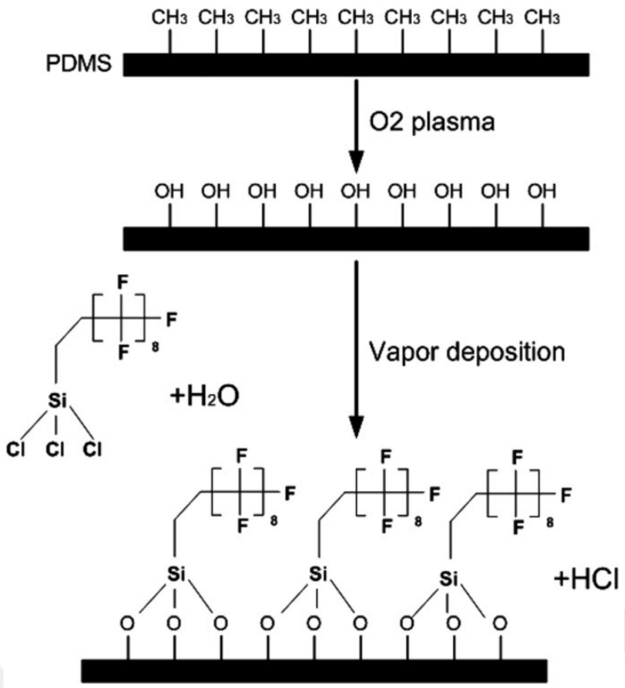

Figure 3.4 Schema of oxygen plasma activation and vapor deposition mechanism of (tridecafluoro-1,1,2,2s-tetrahydrooctyl)trichlorosilane [51]

3.2.3 Preparation of PDMS Replicas via Double Casting Method

PDMS silicone base elastomer and curing agent were mixed in the same proportions (10:1 wt/wt) for all replicas to be obtained using different master molds (M5, M10, and M20). After mixing, the prepolymer was placed in a vacuum desiccator for 45 minutes to degas the air bubbles. Next, the prepolymer was cast on each of the master molds and waited for 60 minutes at room temperature before curing to allow the prepolymer to penetrate the micro-holes. After that, it was cured on hot plates at 70 °C for approximately 4 hours. Finally, after complete curing, each PDMS replica was gently peeled off from the master mold. The fabricated PDMS replicas were coded as shown in Table 3.3. Figure 3.5 shows the fabricated M5, M10, M20, R5, R10, and R20.

For producing a flat replica surface (F10), firstly, a flat master mold was prepared at a 10:1 ratio of silicone base elastomer and curing agent. After that, it was cured at 70 °C for 2 hours after degassing. Then, the aforementioned double-casting protocol was applied.

Table 3.3 Coding of the fabricated PDMS replicas

Replica Code	Meaning of the Code
R5	PDMS replica fabricated using steam annealed M5, which is PDMS master mold with 5:1 wt/wt ratio of base silicone elastomer base and curing agent
R10	PDMS replica fabricated using steam annealed M10, which is PDMS master mold with 10:1 wt/wt ratio of base silicone elastomer base and curing agent
R20	PDMS replica fabricated using steam annealed M20, which is PDMS master mold with 20:1 wt/wt ratio of base silicone elastomer base and curing agent
F10	PDMS replica fabricated using a flat master mold that has a 10:1 wt/wt ratio of base silicone elastomer base and curing agent

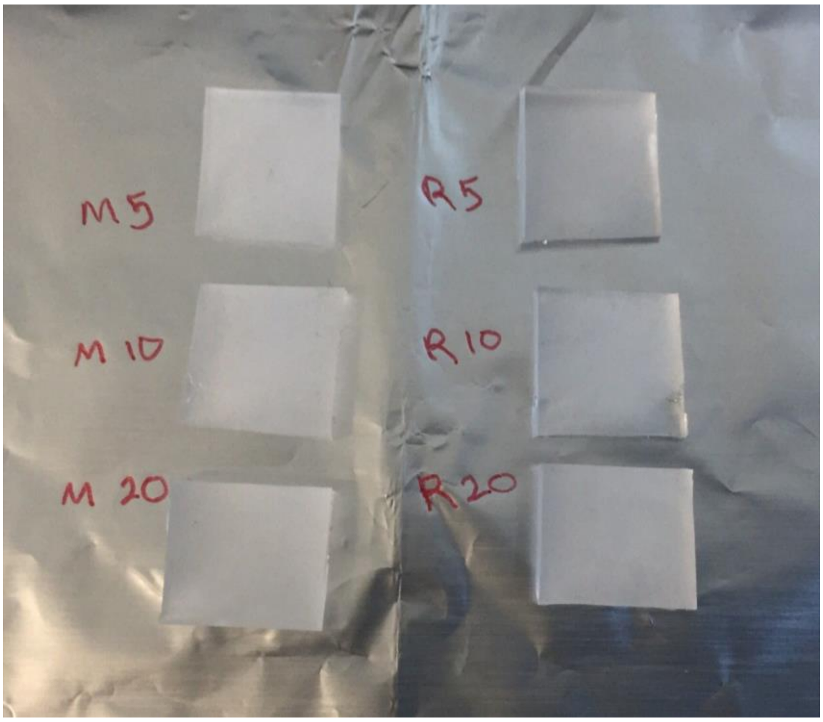

Figure 3.5 The fabricated PDMS master molds and replicas

3.3 Characterization Instruments

3.3.1 Scanning Electron Microscopy (SEM)

SEM is widely used for surface morphology examination. In this study, with the help of SEM instrument in the Department of Materials Science and Engineering at Gebze Technical University (SEM, Philips XL30SFE6), three-dimensional views of steam annealed PDMS master molds and PDMS replicas were obtained. Prior to SEM analysis, the samples were coated with a thin film of gold in order to become electrically conductive and be able to be analyzed.

The hole areas of master molds were calculated using SEM images via the ImageJ program.

3.3.2 Contact Angle Measurement

Wettability examination of steam annealed PDMS master molds with 5:1, 10:1, and 20:1 wt/wt ratio of base silicone elastomer and curing agent and PDMS replicas fabricated using these molds were made via contact angle measurement instrument (KSV CAM200) located in the Department of Chemical Engineering at Gebze Technical University.

With this device (Figure 3.6), the sample's static contact angles and sliding angles of the samples were recorded. For static water contact angle measurements, 5 μl of ultrapure water was dropped on the surface with an automatic needle (dispenser) connected to the device, and the contact angle formed by the water drop on the surface was calculated with the help of the software program on the computer. This measurement was repeated for three different points of the same sample, and the average of the measured values was calculated and reported.

While sliding angle measurement, the sample was placed on a special inclination-adjustable apparatus. By adjusting the surface to a 1° slope, 10 μl of water was dropped onto the surface. If the dropped water did not slide at this inclination, the slope was slightly increased, and the water droplet was dropped again. The smallest angle value at which the water droplet started to move was recorded and determined as the "sliding angle".

Figure 3.6 Contact angle measurement instrument

3.3.3 X-ray Photoelectron Spectroscopy (XPS)

The chemical composition of the replicas obtained by using master molds exposed to fluoro silane gas deposition as an anti-adhesion treatment was examined with the help of the XPS instrument in the Institute of Nanotechnology at Gebze Technical University to determine whether they were affected by this fluoro silane gas or not. For this reason, O 1s, C 1s, F 1s, and Si 2p core lines of each replica were investigated [58]–[61]. A quantitative analysis of XPS data was done via the CasaXPS program to calculate the relative elemental percentage by integrating the area of the fitted core lines.

4
RESULTS AND DISCUSSION

4.1 The Effect of Base Silicone Elastomer and Curing Agent Ratio on Surface Morphology

4.1.1 SEM Images of PDMS Master Molds

The SEM images of the steam annealed PDMS master molds prepared with different base silicone elastomer and curing agent ratios are shown in Figure 4.1. As seen in SEM images, each ratio resulted in different hole sizes. Therefore, we used ImageJ software to calculate hole areas whether there is a significant difference between the holes formed on the surfaces of the master molds.

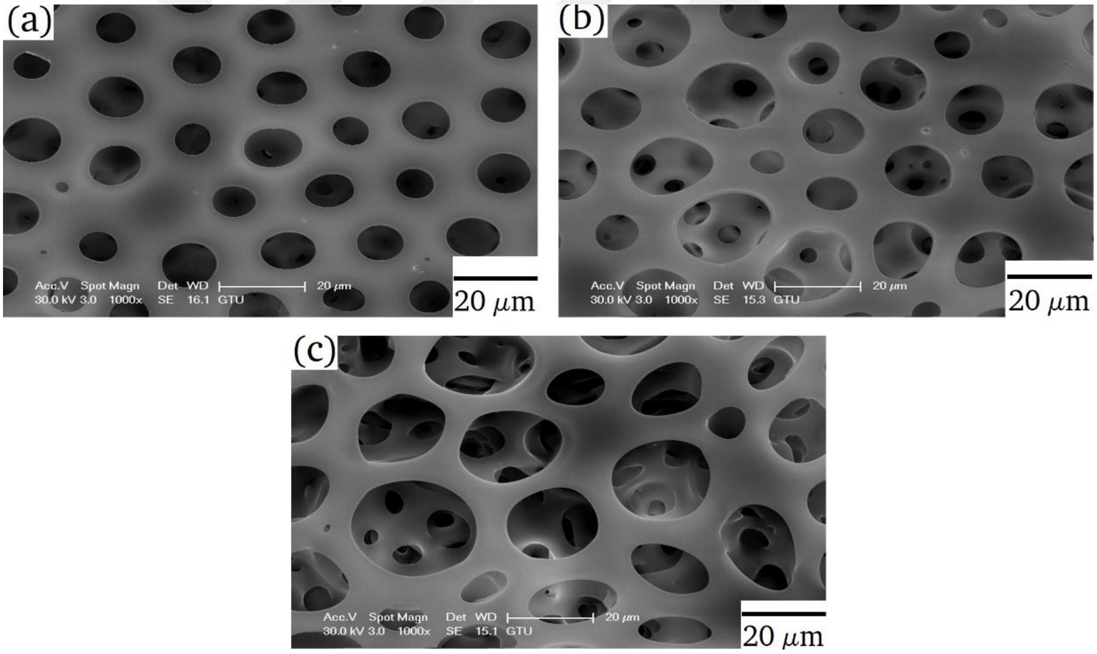

Figure 4.1 SEM images of steam annealed PDMS master molds with base silicone elastomer and curing ratio of (a) 5:1 (b) 10:1 (c) 20:1. The SEM images were taken at 1000x magnification and 30 kV

Figure 4.2 shows the visual steps of calculating the hole areas when using ImageJ. An equal imaging area was used from each sample in this analysis. Table 4.1 reports the analysis data of the holes.

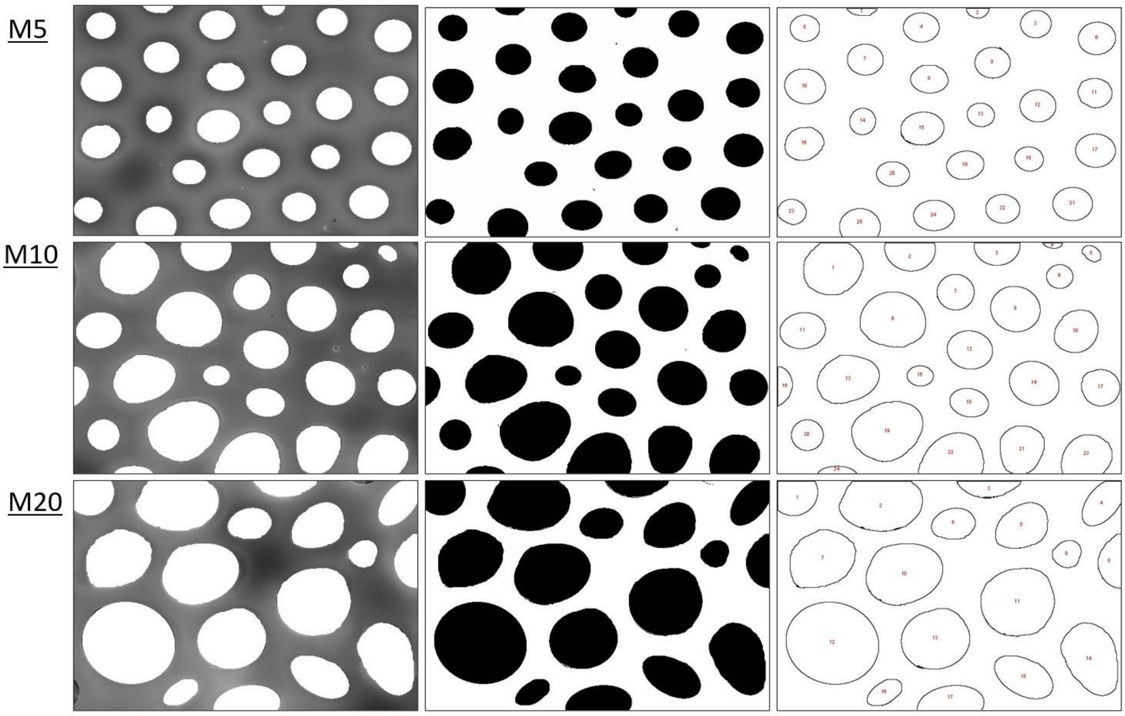

Figure 4.2 Calculating the areas of the micro holes of steam annealed PDMS master molds with ImageJ

Table 4.1 Average areas of micro-holes into steam annealed PDMS master molds calculated via ImageJ program

Master Code	Hole Count	Total Area	Average Size of Holes (μm^2)	%Area
M5	25	2222.88	88.92	24.58
M10	24	3608.23	150.34	39.83
M20	17	4350.05	255.89	48.09

4.1.2 SEM Images of PDMS Replica

The SEM images of fabricated replicas using different master molds were shown in Figure 4.3.

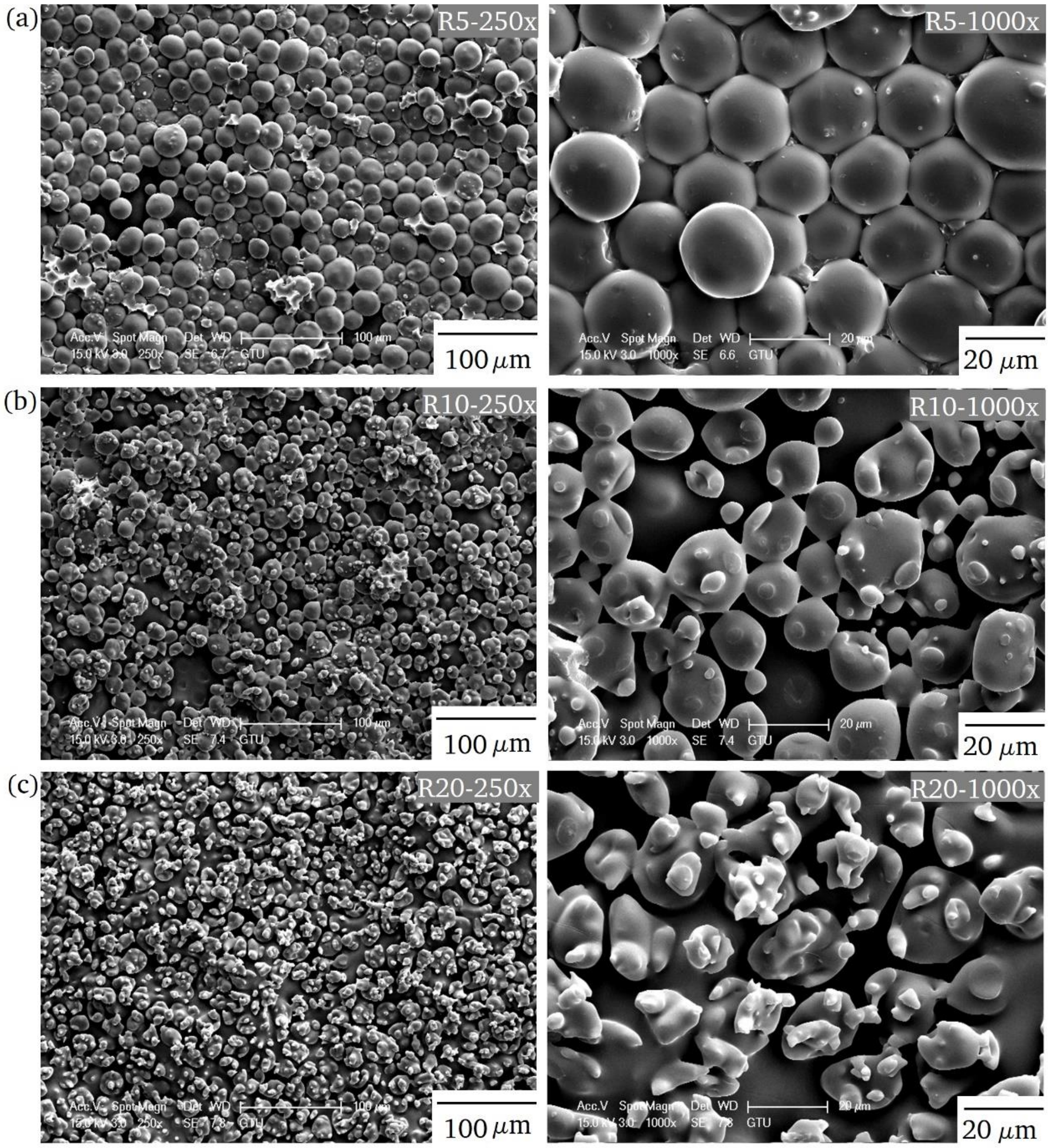

Figure 4.3 SEM images of fabricated PDMS replicas: (a) R5 (b) R10 (c) R20. The SEM images were taken at 250x, 1000x magnifications, and 15 kV

The following outcomes were observed when the SEM images of the steam annealed master molds and their replicas were examined.

- According to SEM images and the calculated average hole sizes, the PDMS master molds prepared at different ratios and subjected to steam annealing have different hole sizes. M5, M10, and M20 have average micro hole areas of 88.92 μm^2, 150.34 μm^2, and 255.8 μm^2, respectively.

- Also, looking at the M5, M10, and M20 SEM images, it is seen that there are secondary holes down the uppermost main holes. However, unlike the M5, the secondary holes in the M10 and M20 are more prominent.
- We can see that the surface of the replica (R5) obtained by using M5 resembles a convex type of irregular honeycomb structure and in the form of bumpy layers.
- Unlike R5, it is seen that the roughness of microstructures on the surfaces of R10 and R20 are denser, resembling lotus leaf-like rough structures.

The first and second observations can be explained as follows: when the master mold that has the highest curing agent ratio, that is prepared with base silicone elastomer and curing agent ratio of 5:1 (M5), is exposed to hot pressurized steam during the steam annealing process, curing occurs faster compared to curing of polymers with 10:1 and 20:1 ratios, and the holes formed on the surface are smaller than the others. Also, this reduces the size and number of secondary holes of M5, as the effect of hot steam on the inner layer will be less during rapid curing. On the other hand, in the master mold with the lowest curing agent ratio (M20), curing takes longer, and hot steam causes larger main holes and more prominent and more numerous secondary holes. In other words, the PDMS curing agent ratio has an inverse relationship with the formed micro hole size. The higher the curing agent ratio, the faster curing during the steam annealing process and the smaller the micro holes. On the contrary, the lower the curing agent ratio, more extended curing and the larger the micro-hole size.

The convex honeycomb-like morphology of R5 can be related to the effect of anti-adhesion treatment. In the fabrication of R5 (Figure 4.4), since the average size of holes of the M5 surface is small, more fluoro silane is retained on the surface when anti-adhesion treatment is applied due to the large PDMS surface area per unit area. This circumstance causes weak leaking of the prepolymer into the holes when poured and remains air gap between the PDMS layers. When the replica is cured, and the master is separated, a shape similar to a convex honeycomb is formed. Similar structures were reported previously in the literature [62], [63].

For example, Uraki et al. [62] obtained a convex-type regular honeycomb-like cellulose structure using polysaccharides.

In M10 and M20 (Figure 4.5 and Figure 4.6), on the other hand, since the total surface area of the holes per the unit area is large, fluoro silane deposited on the PDMS surface will be less. In this way, the PDMS prepolymer not only penetrates within the main holes but also penetrates the secondary holes at the interlayers leading to the formation of hierarchical lotus leaf-like rough replica surfaces. However, it is estimated that the reason for irregular shapes of the R10 and R20 replicas obtained by prepolymer curing is due to the ruptures occurring during the peeling-off process.

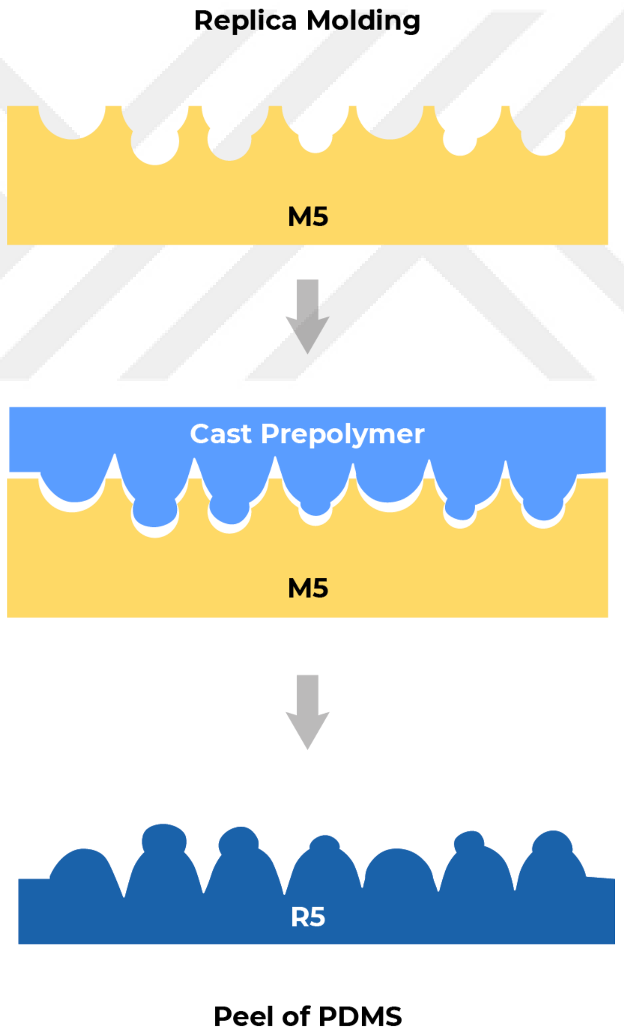

Figure 4.4 Schematic diagrams of soft lithographic replica molding fabrication of R5

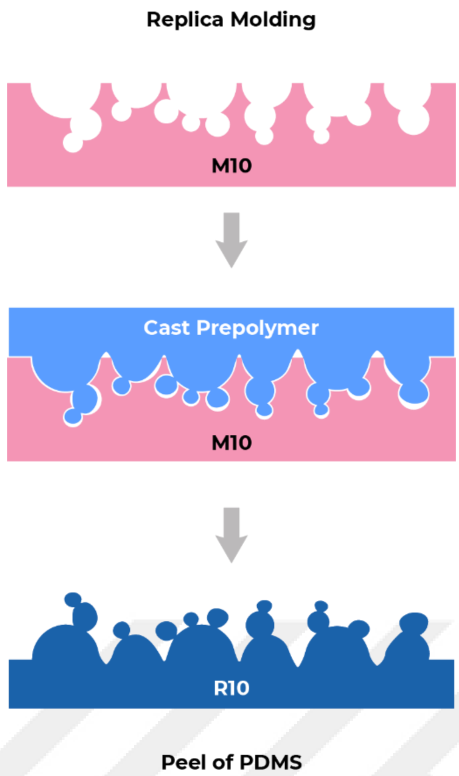

Figure 4.5 Schematic diagrams of soft lithographic replica molding fabrication of R10

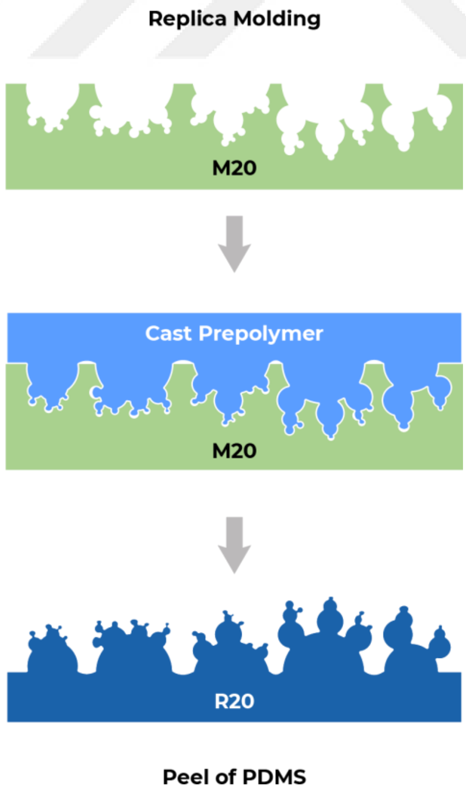

Figure 4.6 Schematic diagrams of soft lithographic replica molding fabrication of R20

To sum up, when replica surfaces are examined, generally it is seen that the microstructures that provide the roughness on the surface are not regular but in the form of bumpy layers. This result is thought to be due to one of the following two possibilities:

i) Since the fluoro silane treatment adds superhydrophobicity to the master molds surfaces, the prepolymer of replicas cannot completely penetrate all the holes, leading to trapping air gaps.

ii) Even if the uncured polymer of the replica completely penetrates the holes, ruptures occur during the peeling-off process, and this causes heterogeneity on the surface.

4.2 The Chemical Composition of Fabricated PDMS Replicas

As mentioned in chapter one, there are two basic approaches to increase the hydrophobicity of a surface: the physical approach, which aims to increase the surface roughness; and the chemical approach, which aims to reduce the surface energy. In some cases, both approaches are used at the same time.

At the beginning of our study, we aimed to increase the roughness of the PDMS surface by adopting the physical approach, which leads to reducing the water-solid contact area and trapping more air pockets between the two phases. However, while fabricating rough PDMS replicas, we questioned whether there is a chemical effect of the gas deposition of fluoro silane that has been used as an anti-adhesive layer or not on the hydrophobicity of final products that directly interact with fluorinated PDMS master molds. To verify this supposition, R5, R10, and R20 were characterized by XPS. The Table 4.2 shows the results of the quantitative analysis, calculated via the CasaXPS and reported as atomic concentrations.

The Figure 4.7 shows the XPS spectra results of R5. It is seen that the element fluorine gives a remarkable peak at around 700 eV [61], [64]. Since it is known that fluorine is not a component of PDMS structure, we can say that it is related to transferred fluorine silane from the master molds, which is (tridecafluoro-1,1,2,2-tetrahydrooctyl) trichlorosilane.

Table 4.2 Elemental analysis (atomic percentage) of fabricated replicas via XPS

Replica Code	C 1s %	F 1s %	O 1s %	Si 2p %
R5	27.37	39.20	20.23	13.21
R10	35.15	28.49	20.49	16.30
R20	28.76	31.66	23.45	16.12

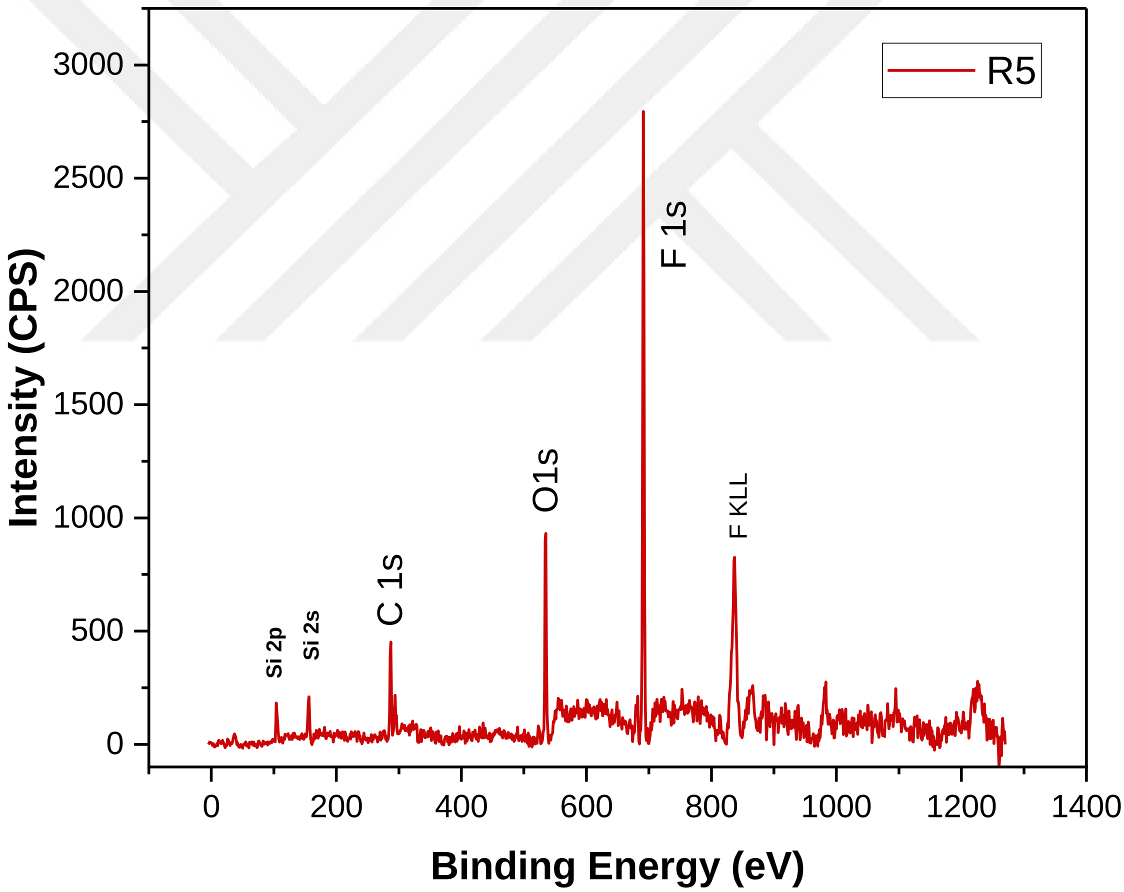

Figure 4.7 XPS spectra for R5

Figure 4.8 and Figure 4.9 also demonstrate the presence of fluorine in R10 and R20, respectively. Previously it has been reported that fluorine-containing treatments grant more hydrophobic surfaces with lower surface energy and lower friction [19], [65]. Our XPS and contact angle measurement results have proven that the fluoro silane treatment influences the master mold surfaces and affects the replicas.

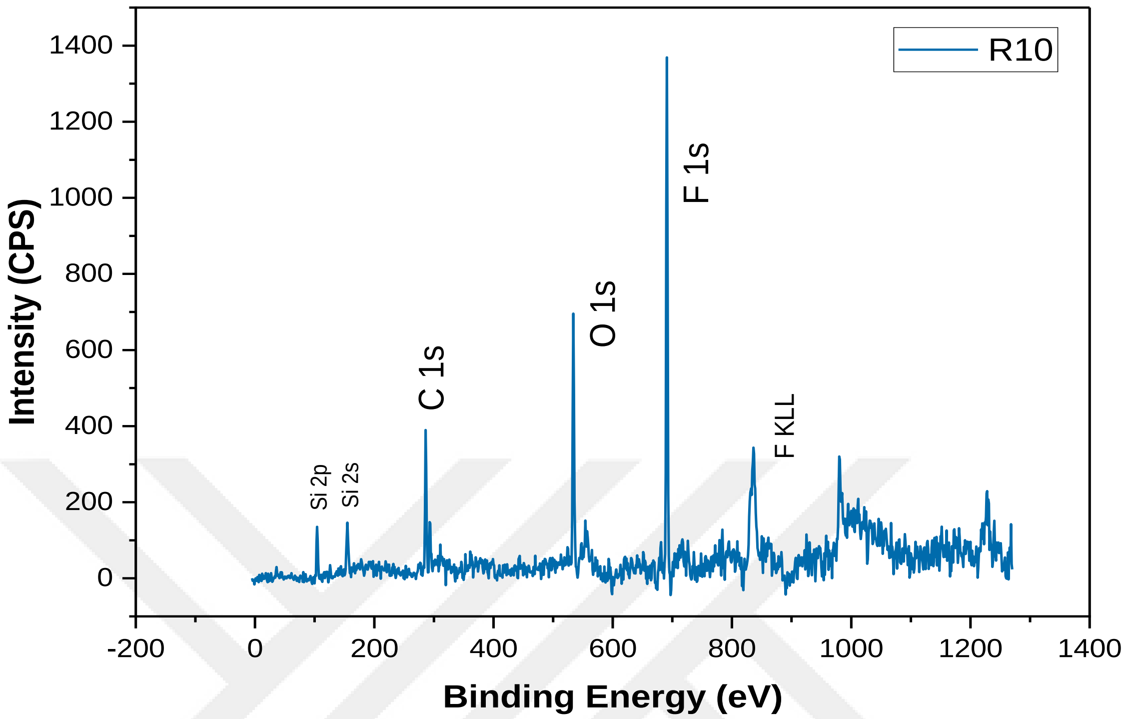

Figure 4.8 XPS spectra for R10

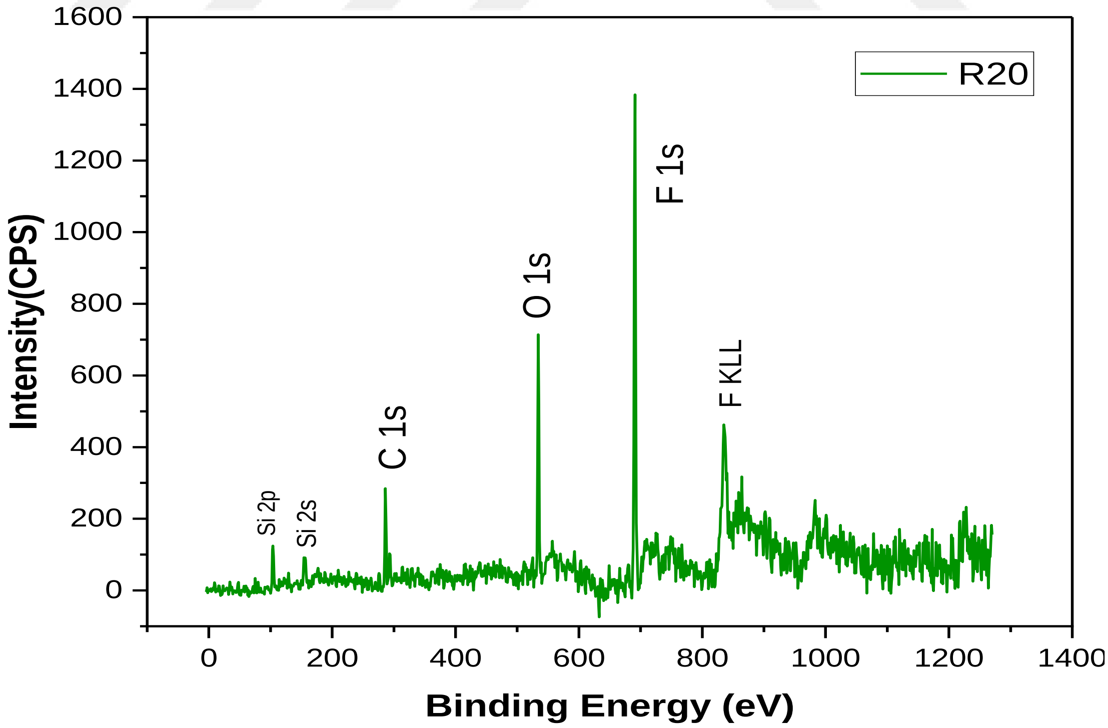

Figure 4.9 XPS spectra for R20

4.3 Contact Angle Measurement Results

4.3.1 Wetting Behavior of Steam Annealed PDMS Master Molds

Figure 4.10 depicts the static contact angle values of master molds. Steam annealed PDMS master molds with 5:1, 10:1, and 20:1 ratio of base silicone elastomer and curing agent have a water contact angle of 124°, 134°, and 148°, respectively. It can be said that the contact angle of water increased with decreasing curing agent ratio in the prepolymer, thereby enhancing the inherent hydrophobicity of PDMS. On the other hand, contact angle measurement of pristine PDMS mold (flat surface) is only 115°.

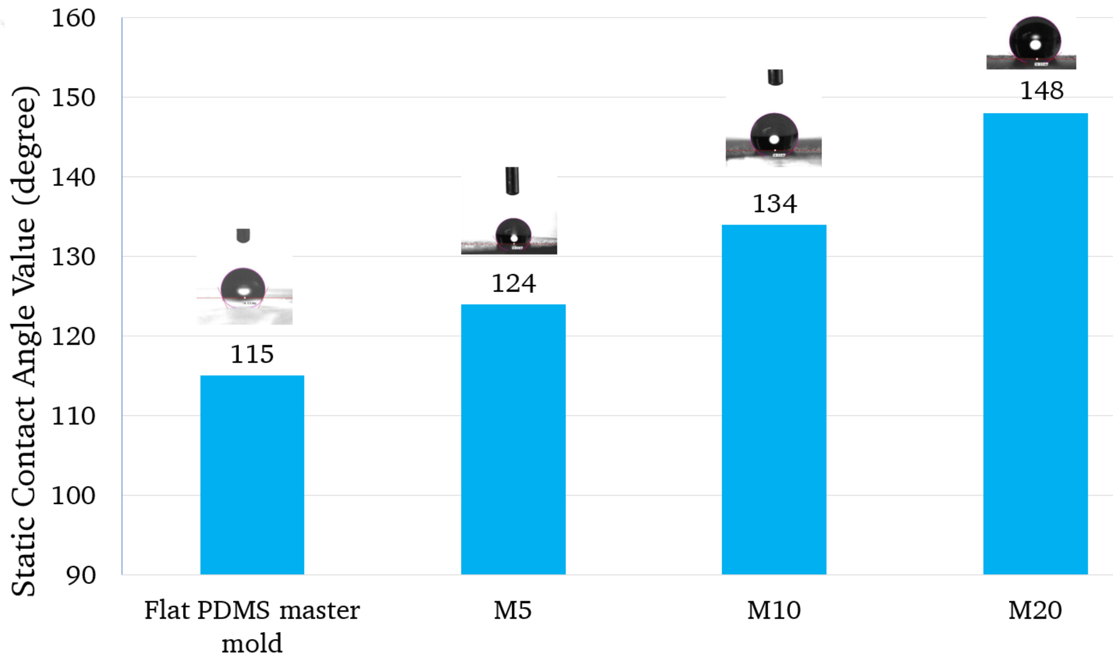

Figure 4.10 Static contact angle values of the flat and steam annealed PDMS master molds

The sliding angle of any master molds could not be measured because the water droplet did not roll down from the surfaces even at 90° of inclination. This behavior indicates that even if the PDMS master molds are more hydrophobic than the flat PDMS they are not showing self-cleaning properties.

4.3.2 Wetting Behavior of PDMS Replica

Comparing the contact angle values of the fabricated replicas and the flat PDMS master mold (Figure 4.11), the pristine PDMS master mold has 115° of water contact angle while F10, flat PDMS replica formed by pristine PDMS mold, has not exceeded 130°. In other words, the flat PDMS replica without roughness could not reach a superhydrophobic level. So, it is clear that although the anti-adhesive fluorinated silane used has led to a slightly positive increase of the hydrophobicity of PDMS replicas, it cannot provide superhydrophobicity by its alone.

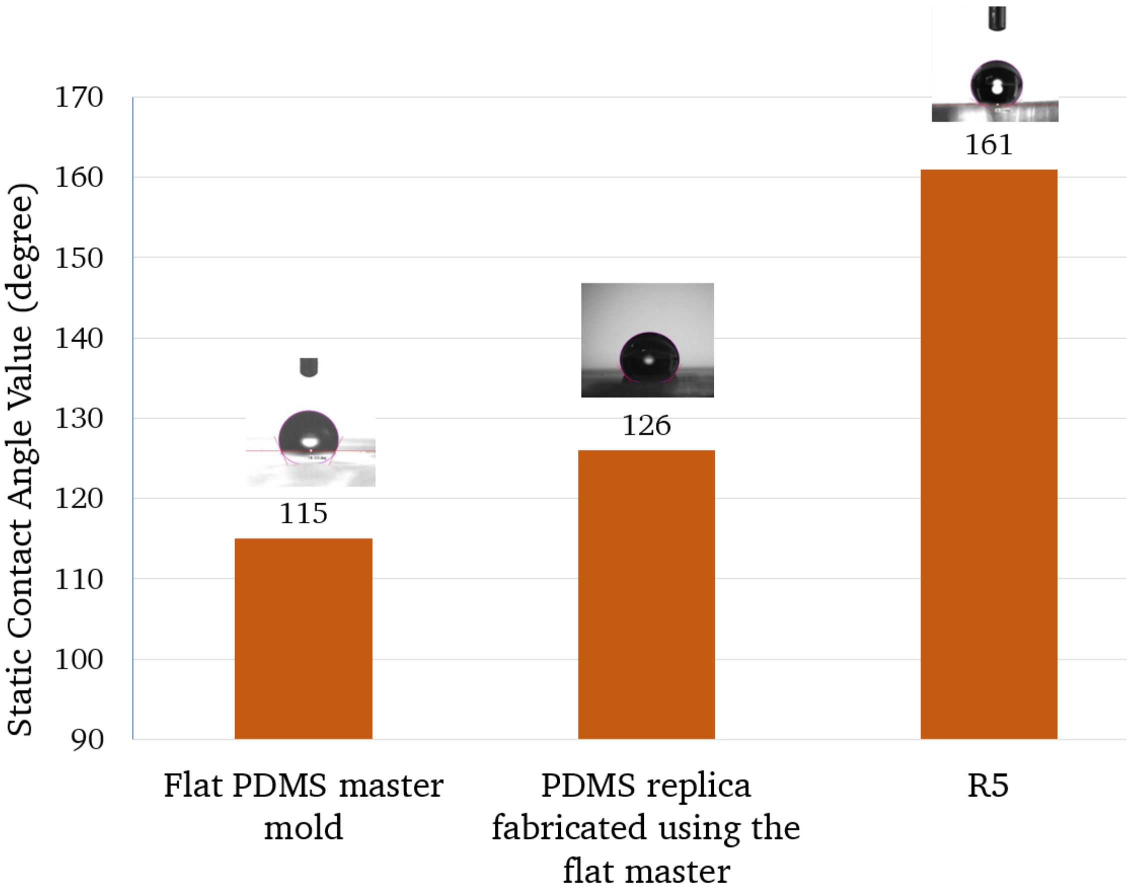

Figure 4.11 Comparing the wettability of the flat PDMS master mold, F10 and R5

Meanwhile, although replica generated from the master mold with a 5:1 ratio has a contact angle larger than 150°, no rolling off occurred while sliding angle measurement. Probably the droplet could not completely stand on the trapped air pockets and partially penetrated between the microstructures on the rough surface, which means the Cassie-Baxter and Wenzel transition module; in other words, the “petal effect” may have occurred [66]. In Table 4.3, the contact angle and sliding angle values of PDMS replicas are given.

Table 4.3 Static water contact angle and sliding angle values of PDMS replica

PDMS Replica	Static Contact Angle Value	Sliding Angle Value
R5	161°	No sliding occurred
R10	>170°	5°
R20	>170°	2°
F10	126°	No sliding occurred

On the other hand, both replicas generated from the master mold with 10:1 and 20:1 ratio had sliding angles less than 10°. While measuring the static angle of these, the droplet did not stand on the surface by any means, which indicates that the surfaces are superhydrophobic having contact angles larger than 170°.

Additionally, when we examined the wettability of replicas in terms of roughness since fluorine was detected in all replicas, it is observed that the sliding angle has decreased as the roughness of the replica surface has increased. R20 has the highest roughness and gives the best performance of self-cleaning property since it has the lowest sliding angle value (~2°).

4.4 Conclusion

This thesis was undertaken to increase the PDMS hydrophobicity by utilizing a soft lithographic double-casting method. The second aim of this study was to investigate the effects of different base silicone elastomer and curing agent ratios on the steam annealed master mold and replicas morphologies.

The surface of a flat PDMS has a contact angle value of 115°, while the produced replica (R20) has a contact angle above 170° and a sliding angle of approximately 2° means that the main aim of this thesis has been achieved.

Other significant findings to emerge from this study are given below.

- The master molds prepared at different ratios and steam annealed have significantly varied hole sizes.

- The master molds with 5:1, 10:1, and 20:1 of base silicone elastomer and curing agent ratio have an average micro hole area of 88.92 μm^2, 150.34 μm^2, and 255.8 μm^2, respectively. These results indicate that while the holes of the master mold with a low curing agent ratio (M20) were large, the holes became smaller as the curing agent ratio increased.
- The roughness of the replicas produced from these master molds has also differed.
- As the average hole size of the master mold surface increased, the roughness of the produced replica also raised.
- The SEM images showed that the roughest replica surface (R20), obtained from the master mold with the least curing agent ratio, has lotus-leaf-like structures.
- Thanks to the XPS and contact angle measurement, it was determined that the fluorine silane used in the soft lithography process did not only chemically bond on the master molds but also transferred to the replica surfaces, causing a slight positive change of water contact angle (~11°).
- The superhydrophobicity properties of produced replicas are due to the combination of both chemical treatment and physical enhancement; it was the result of the actual roughness as well as the effect of the chemical treatment.
- As the roughness of the PDMS replica increased, the sliding angle value decreased, and the droplet rolled more easily from the replica surface.

This study has confirmed the findings of Baek et al. [67], which found that the ratios of base silicone elastomer and curing agent affect the hole density of the steam annealed PDMS surfaces. However, unlike their findings, our results proved that it affects the hole density and affects the hole sizes.

Although the proposed soft lithographic method enhanced the self-cleaning property of PDMS, superhydrophobic surfaces suffer from being incapable of long-term use [68]–[70]. Therefore, further examinations of PDMS microstructures' superhydrophobic behavior under harsh thermal and mechanical conditions are required.

REFERENCES

[1] C. V. Ngo, G. Davaasuren, H. S. Oh, and D. M. Chun, 'Transparency and superhydrophobicity of cone-shaped micropillar array textured polydimethylsiloxane', *Int. J. Precis. Eng. Manuf.*, vol. 16, no. 7, pp. 1347–1353, 2015, doi: 10.1007/s12541-015-0177-z.

[2] F. M. Ma *et al.*, 'Geometrical effect, optimal design and controlled fabrication of bio-inspired micro/nanotextures for superhydrophobic surfaces', *Mater. Res. Express*, vol. 4, no. 9, 2017, doi: 10.1088/2053-1591/aa7d23.

[3] Z. Pan, F. Cheng, and B. Zhao, 'Bio-Inspired polymeric structures with special wettability and their applications: An overview', *Polymers (Basel).*, vol. 9, no. 12, pp. 32–39, 2017, doi: 10.3390/polym9120725.

[4] A. Hussain, A. Batra, and R. Pachauri, 'An experimental study on effect of dust on power loss in solar photovoltaic module', *Renewables Wind. Water, Sol.*, vol. 4, no. 1, 2017, doi: 10.1186/s40807-017-0043-y.

[5] U. Mehmood, F. A. Al-Sulaiman, B. S. Yilbas, B. Salhi, S. H. A. Ahmed, and M. K. Hossain, 'Superhydrophobic surfaces with antireflection properties for solar applications: A critical review', *Sol. Energy Mater. Sol. Cells*, vol. 157, pp. 604–623, 2016, doi: 10.1016/j.solmat.2016.07.038.

[6] J. Yoon *et al.*, 'Wet-Style Superhydrophobic Antifogging Coatings for Optical Sensors', *Adv. Mater.*, vol. 32, no. 34, pp. 1–7, 2020, doi: 10.1002/adma.202002710.

[7] L. B. Boinovich, A. M. Emelyanenko, K. A. Emelyanenko, and K. I. Maslakov, 'Anti-icing properties of a superhydrophobic surface in a salt environment: An unexpected increase in freezing delay times for weak brine droplets', *Phys. Chem. Chem. Phys.*, vol. 18, no. 4, pp. 3131–3136, 2016, doi: 10.1039/c5cp06988b.

[8] W. Liu, H. Chen, Y. Shen, and Z. Wu, 'Facilely Fabricating Superhydrophobic Resin-based Coatings with Lower Water Freezing Temperature and Ice Adhesion for Anti-icing Application', *J. Bionic Eng.*, vol. 16, no. 5, pp. 794–805, 2019, doi: 10.1007/s42235-019-0097-1.

[9] J. Yeo, M. J. Choi, and D. S. Kim, 'Robust hydrophobic surfaces with various micropillar arrays', *J. Micromechanics Microengineering*, vol. 20, no. 2, 2010, doi: 10.1088/0960-1317/20/2/025028.

[10] K. M. Lee, C. V. Ngo, J. Y. Jeong, E. chae Jeon, T. J. Je, and D. M. Chun, 'Fabrication of an anisotropic superhydrophobic polymer surface using compression molding and dip coating', *Coatings*, vol. 7, no. 11, 2017, doi: 10.3390/coatings7110194.

[11] K. Maghsoudi, E. Vazirinasab, G. Momen, and R. Jafari, 'Advances in the Fabrication of Superhydrophobic Polymeric Surfaces by Polymer Molding Processes', *Ind. Eng. Chem. Res.*, vol. 59, no. 20, pp. 9343–9363, 2020, doi:

10.1021/acs.iecr.0c00508.

[12] C. E. Cansoy, H. Y. Erbil, O. Akar, and T. Akin, 'Effect of pattern size and geometry on the use of Cassie-Baxter equation for superhydrophobic surfaces', *Colloids Surfaces A Physicochem. Eng. Asp.*, vol. 386, no. 1–3, pp. 116–124, 2011, doi: 10.1016/j.colsurfa.2011.07.005.

[13] J. Jeevahan, M. Chandrasekaran, G. Britto Joseph, R. B. Durairaj, and G. Mageshwaran, 'Superhydrophobic surfaces: a review on fundamentals, applications, and challenges', *J. Coatings Technol. Res.*, vol. 15, no. 2, pp. 231–250, 2018, doi: 10.1007/s11998-017-0011-x.

[14] J. Wang, Y. Wu, Y. Cao, G. Li, and Y. Liao, 'Influence of surface roughness on contact angle hysteresis and spreading work', *Colloid Polym. Sci.*, vol. 298, no. 8, pp. 1107–1112, 2020, doi: 10.1007/s00396-020-04680-x.

[15] S. Rasouli, N. Rezaei, H. Hamedi, S. Zendehboudi, and X. Duan, 'Superhydrophobic and superoleophilic membranes for oil-water separation application: A comprehensive review', *Mater. Des.*, vol. 204, p. 109599, 2021, doi: 10.1016/j.matdes.2021.109599.

[16] J. Gao, J. Zhao, L. Liu, and W. Xue, 'Dimensional effects of polymer pillar arrays on hydrophobicity', *Surf. Eng.*, vol. 32, no. 2, pp. 125–131, 2016, doi: 10.1179/1743294414Y.0000000431.

[17] S. Martin and B. Bhushan, 'Transparent, wear-resistant, superhydrophobic and superoleophobic poly(dimethylsiloxane) (PDMS) surfaces', *J. Colloid Interface Sci.*, vol. 488, pp. 118–126, 2017, doi: 10.1016/j.jcis.2016.10.094.

[18] W. Jia, J. A. Kharraz, P. J. Choi, J. Guo, B. J. Deka, and A. K. An, 'Superhydrophobic membrane by hierarchically structured PDMS-POSS electrospray coating with cauliflower-shaped beads for enhanced MD performance', *J. Memb. Sci.*, vol. 597, no. October 2019, p. 117638, 2020, doi: 10.1016/j.memsci.2019.117638.

[19] A. Ansari, R. Trehan, C. Watson, and S. Senyo, 'Increasing silicone mold longevity: a review of surface modification techniques for PDMS-PDMS double casting.', *Soft Mater.*, vol. 00, no. 00, pp. 1–12, 2020, doi: 10.1080/1539445X.2020.1850476.

[20] M. J. Madou, *Fundamentals of Microfabrication and Nanotechnology, Three-Volume Set*. CRC Press, 2018.

[21] O. Sahin, M. Ashokkumar, and P. M. Ajayan, *3. Micro- and nanopatterning of biomaterial surfaces*, no. i. Woodhead Publishing, 2018.

[22] P. S. Brown and B. Bhushan, 'Bioinspired materials for water supply and management: Water collection, water purification and separation of water from oil', *Philos. Trans. R. Soc. A Math. Phys. Eng. Sci.*, vol. 374, no. 2073, 2016, doi: 10.1098/rsta.2016.0135.

[23] N. Nuraje, W. S. Khan, Y. Lei, M. Ceylan, and R. Asmatulu, 'Superhydrophobic electrospun nanofibers', *J. Mater. Chem. A*, vol. 1, no. 6, pp. 1929–1946, 2013, doi: 10.1039/c2ta00189f.

[24] C. Neinhuis and W. Barthlott, 'Characterization and distribution of water-

repellent, self-cleaning plant surfaces', *Ann. Bot.*, vol. 79, no. 6, pp. 667–677, 1997, doi: 10.1006/anbo.1997.0400.

[25] B. Bhushan and Y. C. Jung, 'Natural and biomimetic artificial surfaces for superhydrophobicity, self-cleaning, low adhesion, and drag reduction', *Prog. Mater. Sci.*, vol. 56, no. 1, pp. 1–108, 2011, doi: 10.1016/j.pmatsci.2010.04.003.

[26] J. Zhang *et al.*, 'How does the leaf margin make the lotus surface dry as the lotus leaf floats on water?', *Soft Matter*, vol. 4, no. 11, pp. 2232–2237, 2008, doi: 10.1039/b807857b.

[27] B. B. and M. Nosonovsky, *Rose Petal Effect. In: Bhushan B. (eds) Encyclopedia of Nanotechnology.* Dordrecht: Springer, 2012.

[28] T. Kong, G. Luo, Y. Zhao, and Z. Liu, 'Bioinspired Superwettability Micro/Nanoarchitectures: Fabrications and Applications', *Adv. Funct. Mater.*, vol. 29, no. 11, pp. 1–32, 2019, doi: 10.1002/adfm.201808012.

[29] M. N. MacGregor-Ramiasa and K. Vasilev, 'Questions and Answers on the Wettability of Nano-Engineered Surfaces', *Adv. Mater. Interfaces*, vol. 4, no. 16, pp. 1–24, 2017, doi: 10.1002/admi.201700381.

[30] M. Villegas, Y. Zhang, N. Abu Jarad, L. Soleymani, and T. F. Didar, 'Liquid-Infused Surfaces: A Review of Theory, Design, and Applications', *ACS Nano*, vol. 13, no. 8, pp. 8517–8536, 2019, doi: 10.1021/acsnano.9b04129.

[31] T. Betancourt and L. Brannon-Peppas, 'Micro-and nanofabrication methods in nanotechnological medical and pharmaceutical devices', *Int. J. Nanomedicine*, vol. 1, no. 4, pp. 483–495, 2006, doi: 10.2147/nano.2006.1.4.483.

[32] M. Tang, V. Shim, Z. Y. Pan, Y. S. Choo, and M. H. Hong, 'Laser ablation of metal substrates for super-hydrophobic effect', *J. Laser Micro Nanoeng.*, vol. 6, no. 1, pp. 6–9, 2011, doi: 10.2961/jlmn.2011.01.0002.

[33] J. Yang, H. Li, T. Lan, L. Peng, R. Cui, and H. Yang, 'Preparation, characterization, and properties of fluorine-free superhydrophobic paper based on layer-by-layer assembly', *Carbohydr. Polym.*, vol. 178, no. June, pp. 228–237, 2017, doi: 10.1016/j.carbpol.2017.09.040.

[34] M. Long *et al.*, 'Robust and thermal-healing superhydrophobic surfaces by spin-coating of polydimethylsiloxane', *J. Colloid Interface Sci.*, vol. 508, pp. 18–27, 2017, doi: 10.1016/j.jcis.2017.08.027.

[35] N. Celik, I. Torun, M. Ruzi, A. Esidir, and M. S. Onses, 'Fabrication of robust superhydrophobic surfaces by one-step spray coating: Evaporation driven self-assembly of wax and nanoparticles into hierarchical structures', *Chem. Eng. J.*, vol. 396, no. December 2019, p. 125230, 2020, doi: 10.1016/j.cej.2020.125230.

[36] K. M. Lee, H. Park, J. Kim, and D. M. Chun, 'Fabrication of a superhydrophobic surface using a fused deposition modeling (FDM) 3D printer with poly lactic acid (PLA) filament and dip coating with silica nanoparticles', *Appl. Surf. Sci.*, vol. 467–468, no. September 2018, pp. 979–

991, 2019, doi: 10.1016/j.apsusc.2018.10.205.

[37] D. J. Lipomi, R. V. Martinez, L. Cademartiri, and G. M. Whitesides, *Soft Lithographic Approaches to Nanofabrication*, vol. 7. Elsevier B.V., 2012.

[38] B. Liu, Y. He, Y. Fan, and X. Wang, 'Fabricating super-hydrophobie lotus-leaf-like surfaces through soft-lithographic imprinting', *Macromol. Rapid Commun.*, vol. 27, no. 21, pp. 1859–1864, 2006, doi: 10.1002/marc.200600492.

[39] M. Mayhoub, 'Cleaning innovative daylighting systems: Review and suggested methods', *Light. Res. Technol.*, vol. 49, no. 8, pp. 1015–1033, 2017, doi: 10.1177/1477153516669969.

[40] S. M. Kang, N. Ahn, J. W. Lee, M. Choi, and N. G. Park, 'Water-repellent perovskite solar cell', *J. Mater. Chem. A*, vol. 2, no. 47, pp. 20017–20021, 2014, doi: 10.1039/c4ta05413j.

[41] B. Zhang, J. Wang, and J. Zhang, 'Bioinspired one step hydrothermal fabricated superhydrophobic aluminum alloy with favorable corrosion resistance', *Colloids Surfaces A Physicochem. Eng. Asp.*, vol. 589, no. 7, p. 124469, 2020, doi: 10.1016/j.colsurfa.2020.124469.

[42] S. Abbasi, M. Nouri, and A. Sabour Rouhaghdam, 'A novel combined method for fabrication of stable corrosion resistance superhydrophobic surface on Al alloy', *Corros. Sci.*, vol. 159, no. August, p. 108144, 2019, doi: 10.1016/j.corsci.2019.108144.

[43] J. Kuang, Z. Ba, Z. Li, Y. Jia, and Z. Wang, 'Fabrication of a superhydrophobic Mg-Mn layered double hydroxides coating on pure magnesium and its corrosion resistance', *Surf. Coatings Technol.*, vol. 361, no. January, pp. 75–82, 2019, doi: 10.1016/j.surfcoat.2019.01.009.

[44] S. Dong *et al.*, 'Construction and corrosion resistance of Ni-B4C superhydrophobic composite coatings on Q235 steel', *Surf. Coatings Technol.*, vol. 422, no. July, p. 127551, 2021, doi: 10.1016/j.surfcoat.2021.127551.

[45] Z. Shao, Y. Wang, and H. Bai, 'A superhydrophobic textile inspired by polar bear hair for both in air and underwater thermal insulation', *Chem. Eng. J.*, vol. 397, no. May, p. 125441, 2020, doi: 10.1016/j.cej.2020.125441.

[46] Z. Ye, S. Li, S. Zhao, L. Deng, J. Zhang, and A. Dong, 'Textile coatings configured by double-nanoparticles to optimally couple superhydrophobic and antibacterial properties', *Chem. Eng. J.*, vol. 420, no. P2, p. 127680, 2021, doi: 10.1016/j.cej.2020.127680.

[47] P. K. Sow, R. Singhal, P. Sahoo, and S. Radhakanth, 'Fabricating low-cost, robust superhydrophobic coatings with re-entrant topology for self-cleaning, corrosion inhibition, and oil-water separation', *J. Colloid Interface Sci.*, vol. 600, pp. 358–372, 2021, doi: 10.1016/j.jcis.2021.05.026.

[48] G. S. Jeong *et al.*, 'Solderable and electroplatable flexible electronic circuit on a porous stretchable elastomer', *Nat. Commun.*, vol. 3, no. May, 2012, doi: 10.1038/ncomms1980.

[49] J. Jung, M. Nakajima, M. Takeuchi, Z. Najdovski, Q. Huang, and T. Fukuda, ‘Microfluidic Device to Measure the Speed of C. elegans Using the Resistance Change of the Flexible Electrode’, *Micromachines*, vol. 7, no. 3, p. 50, Mar. 2016, doi: 10.3390/mi7030050.

[50] Y. J. Yun *et al.*, ‘Highly Elastic Graphene-Based Electronics Toward Electronic Skin’, *Adv. Funct. Mater.*, vol. 27, no. 33, 2017, doi: 10.1002/adfm.201701513.

[51] G. Zhuang and J. P. Kutter, ‘Anti-stiction coating of PDMS moulds for rapid microchannel fabrication by double replica moulding’, *J. Micromechanics Microengineering*, vol. 21, no. 10, 2011, doi: 10.1088/0960-1317/21/10/105020.

[52] Y. L. Deng and Y. J. Juang, ‘Polydimethyl siloxane wet etching for three dimensional fabrication of microneedle array and high-aspect-ratio micropillars’, *Biomicrofluidics*, vol. 8, no. 2, pp. 1–6, 2014, doi: 10.1063/1.4871038.

[53] G. Shao, J. Wu, Z. Cai, and W. Wang, ‘Fabrication of elastomeric high-aspect-ratio microstructures using polydimethylsiloxane (PDMS) double casting technique’, *Sensors Actuators, A Phys.*, vol. 178, pp. 230–236, 2012, doi: 10.1016/j.sna.2012.01.034.

[54] R. Soffe, M. Bernach, M. N. P. Remus-Emsermann, and V. Nock, ‘Replicating Arabidopsis Model Leaf Surfaces for Phyllosphere Microbiology’, *Sci. Rep.*, vol. 9, no. 1, pp. 1–12, 2019, doi: 10.1038/s41598-019-50983-7.

[55] B. Bhushan, D. Hansford, and K. K. Lee, ‘Surface modification of silicon and polydimethylsiloxane surfaces with vapor-phase-deposited ultrathin fluorosilane films for biomedical nanodevices’, *J. Vac. Sci. Technol. A Vacuum, Surfaces, Film.*, vol. 24, no. 4, pp. 1197–1202, 2006, doi: 10.1116/1.2167077.

[56] S. H. Tan, N. T. Nguyen, Y. C. Chua, and T. G. Kang, ‘Oxygen plasma treatment for reducing hydrophobicity of a sealed polydimethylsiloxane microchannel’, *Biomicrofluidics*, vol. 4, no. 3, pp. 1–8, 2010, doi: 10.1063/1.3466882.

[57] B. Ruben *et al.*, ‘Oxygen plasma treatments of polydimethylsiloxane surfaces: Effect of the atomic oxygen on capillary flow in the microchannels’, *Micro Nano Lett.*, vol. 12, no. 10, pp. 754–757, 2017, doi: 10.1049/mnl.2017.0230.

[58] P. Guida *et al.*, ‘Enhancing miRNAs Capture on Polydimethylsiloxane Surface with Nanostructuration’, *J. Nanomed. Nanotechnol.*, vol. 08, no. 02, 2017, doi: 10.4172/2157-7439.1000437.

[59] M. Zhang, J. Wu, L. Wang, K. Xiao, and W. Wen, ‘A simple method for fabricating multi-layer PDMS structures for 3D microfluidic chips’, *Lab Chip*, vol. 10, no. 9, pp. 1199–1203, 2010, doi: 10.1039/b923101c.

[60] Z. He *et al.*, ‘Fabrication of a transparent superamphiphobic coating with improved stability’, *Soft Matter*, vol. 7, no. 14, pp. 6435–6443, 2011, doi: 10.1039/c1sm05574g.

[61] Z. Pan, H. Shahsavan, W. Zhang, F. K. Yang, and B. Zhao, 'Superhydro-oleophobic bio-inspired polydimethylsiloxane micropillared surface via FDTS coating/blending approaches', *Appl. Surf. Sci.*, vol. 324, pp. 612–620, 2015, doi: 10.1016/j.apsusc.2014.10.146.

[62] Y. Uraki, Y. Tamai, T. Hirai, K. Koda, H. Yabu, and M. Shimomura, 'Fabrication of honeycomb-patterned cellulose material that mimics wood cell wall formation processes', *Mater. Sci. Eng. C*, vol. 31, no. 6, pp. 1201–1208, 2011, doi: 10.1016/j.msec.2010.11.009.

[63] H. K. Choi, M. H. Kim, S. H. Im, and O. O. Park, 'Fabrication of ordered nanostructured arrays using poly(dimethylsiloxane) replica molds based on three-dimensional colloidal crystals', *Adv. Funct. Mater.*, vol. 19, no. 10, pp. 1594–1600, 2009, doi: 10.1002/adfm.200801096.

[64] W. Tang, Y. Huang, W. Meng, and F. L. Qing, 'Synthesis of fluorinated hyperbranched polymers capable as highly hydrophobic and oleophobic coating materials', *Eur. Polym. J.*, vol. 46, no. 3, pp. 506–518, 2010, doi: 10.1016/j.eurpolymj.2009.12.005.

[65] T. Kasai, B. Bhushan, G. Kulik, L. Barbieri, and P. Hoffmann, 'Micro⁄nanotribological study of perfluorosilane SAMs for antistiction and low wear', *J. Vac. Sci. Technol. B Microelectron. Nanom. Struct.*, vol. 23, no. 3, p. 995, 2005, doi: 10.1116/1.1913674.

[66] J. Geils, G. Patzelt, and A. Kesel, 'The larger the contact angle , the lower the adhesion?', in *Bionik Pat. Aus Der Natur. Innov. Für Technol.*, 2019, pp. 188–195.

[67] D. H. Baek *et al.*, 'Effect of viscosity on the formation of porous polydimethylsiloxane for wearable device applications', *Molecules*, vol. 26, no. 5, pp. 1–8, 2021, doi: 10.3390/molecules26051471.

[68] R. Sharma, S. S. Das, U. U. Ghosh, S. DasGupta, and S. Chakraborty, 'Pitcher Plant Inspired Biomimetic Liquid Infused Slippery Surface Using Taro Leaf', 2018, [Online]. Available: http://arxiv.org/abs/1812.10368.

[69] E. Kasapgil, I. Anac, and H. Y. Erbil, 'Transparent, fluorine-free, heat-resistant, water repellent coating by infusing slippery silicone oil on polysiloxane nanofilament layers prepared by gas phase reaction of n-propyltrichlorosilane and methyltrichlorosilane', *Colloids Surfaces A Physicochem. Eng. Asp.*, vol. 560, no. July 2018, pp. 223–232, 2019, doi: 10.1016/j.colsurfa.2018.09.064.

[70] T. S. Wong *et al.*, 'Bioinspired self-repairing slippery surfaces with pressure-stable omniphobicity', *Nature*, vol. 477, no. 7365, pp. 443–447, 2011, doi: 10.1038/nature10447.

PUBLICATIONS FROM THE THESIS

Conference Papers

1. M. Akraa, H. Sadikoglu, M.E. Oruc, and S. Omeroglu "Hydrophobicity of Fabricated Polydimethylsiloxane (PDMS) Microstructures", presented at the 5^{th} International Congress on Engineering and Technology Management, Istanbul, April 2021.